ACS Chemical Neuroscience

pubs.acs.org/chemneuro Research Article

Isodrimenine Derivatives Selectively Inhibit Human α7-Containing Nicotinic Acetylcholine Receptors via Negative Allosteric Modulation

Han-Shen Tae,* Marcelo O. Ortells, Alexandru Ciocarlan, Aculina Aricu, Lidia Lungu, Svetlana Blaja, David J. Adams, and Hugo R. Arias

Cite This: ACS Chem. Neurosci. 2026, 17, 260−274 Read Online

ACCESS | Metrics & More | Article Recommendations

ABSTRACT: Drimane sesquiterpenoids are biologically active compounds found in plants, fungi, and marine organisms. Three isodrimenine derivatives, 5,6-dehydro-7-keto-isodrimenine (DH7KID), 7-keto-isodrimenine (7KID), and 7-acetoxy-isodrimenine (7AID), belonging to the drimane-type sesquiterpene family were synthesized and evaluated for activity at various human nicotinic acetylcholine receptor (nAChR) subtypes using two-electrode voltage-clamp electrophysiology. All three compounds exhibited comparable inhibitory potency across nAChR subtypes but showed greater selectively for α7-containing receptors. For DH7KID, the selectivity order was $\alpha7\beta2 \cong \alpha7 > \alpha4\beta4 > \alpha6^*\beta2\beta3$ (*α6-α3 chimera) $> \alpha4\beta2 \cong \alpha6^*\beta4 > \alpha3\beta4 \cong \alpha3\beta2 > \alpha9\alpha10$. Inhibition of α7 and α4β4 nAChRs by DH7KID and 7KID, respectively, was independent of acetylcholine concentration, indicating a noncompetitive mechanism and suggesting that these compounds do not act at the orthosteric site. Furthermore, inhibition was voltage-independent, consistent with binding to a nonluminal allosteric site. The deactivation time constants of currents mediated by α7- and α4-containing nAChRs were unaffected by isodrimenine. *In silico* structural analyses further supported the interaction of DH7KID with nonluminal allosteric sites on the α7 nAChR. Collectively, these findings demonstrate that isodrimenine derivatives function as negative allosteric modulators of α7-containing nAChRs. Given the biological significance of α7 nAChRs, isodrimenine-induced inhibition may have therapeutic relevance for neuropsychiatric disorders.

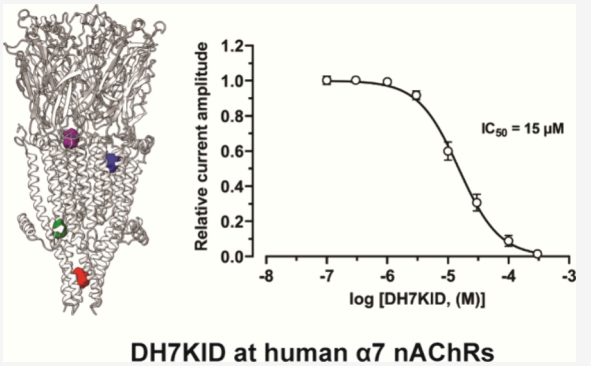

KEYWORDS: *drimane sesquiterpenoid, isodrimenine, nicotinic acetylcholine receptor, electrophysiology, molecular docking, negative allosteric modulation*

1. INTRODUCTION

Drimane sesquiterpenoids are a large class of natural compounds found in plants, fungi, and marine organisms, many of which exhibit diverse biological activities.[1] Natural compounds such as polygodial, warburganal, cinnamodial, cinnamosmolide, and pereniporins A and B, along with their synthetic derivatives, including nitrogen-containing analogues, display antibacterial, antifungal, and anticancer activities.[1,2] These properties highlight their potential for clinical application and justify continued investigation. More recently, research has focused on developing molecular hybrids of drimane sesquiterpenoids, with heterocyclic structural motifs such as azaheterocycles, 1,3-benzothiazoles, and benzimidazoles, an area showing promising progress.[3−5]

Isodrimenine derivatives have attracted significant attention due to their diverse pharmacological activities. They function as agonists at the nonselective transient receptor potential ankyrin 1 (TRPA1) ion channel and inhibit the expression of proteins involved in intracellular signaling pathways, including PI3K/Akt/GSK3β, as well as mitochondrial ATP synthesis.[2] Our laboratory has previously investigated several drimane sesquiterpenoids, including drimenine and cinnamolide, for their activity at human (h) nicotinic acetylcholine receptors (nAChRs) using Ca^{2+}-induced fluorescence imaging.[6] These compounds were shown to act as noncompetitive inhibitors of nAChRs, exhibiting greater potency at the α4β2 subtype than at α3β4 or α7 nAChRs. However, it remains unclear whether structurally distinct drimane derivatives can modulate other

Received: November 3, 2025
Revised: December 3, 2025
Accepted: December 5, 2025
Published: December 17, 2025

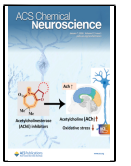

https://doi.org/10.1021/acschemneuro.5c00862
ACS Chem. Neurosci. 2026, 17, 260−274

nAChR subtypes or if they operate through different molecular mechanisms.

To address this question, we synthesized three isodrimenine derivatives, 5,6-dehydro-7-keto-isodrimenine (DH7KID), 7-keto-isodrimenine (7KID), and 7-acetoxy-isodrimenine (7AID), each containing a keto or acetoxy substituent at the C_7 position, which is absent in drimenine (Figure 1).[6] We

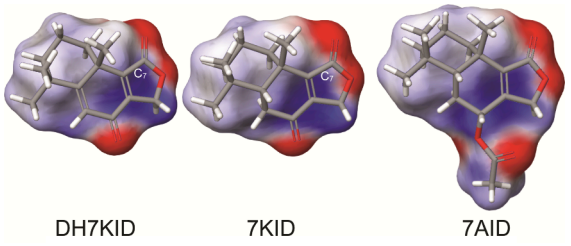

Figure 1. Molecular structures of 5,6-dehydro-7-keto-isodrimenine (9) (DH7KID), 7-keto-isodrimenine (10) (7KID), and 7-acetoxy-isodrimenine (12) (7AID). Molecules are shown in stick representation and colored by atom (C gray, O red, H white), superposed on their electrostatic potential surfaces (red, more negative; blue, more positive). The C_7 position, where hydrogen bond acceptors are located, is indicated. Images were generated using Schrödinger Maestro.

evaluated their activity across multiple human nAChR subtypes expressed in *Xenopus laevis* oocytes using two-electrode voltage-clamp electrophysiology and identified selective inhibitory effects on hα7-containing nAChRs. Given previous studies have shown that α7 nAChR inhibition produces antidepressant-, anxiolytic-, and promnesic-like effects, as well as alleviates attentional deficits in rodents,[7−11] we further investigated the mechanism of inhibition at this subtype. Specifically, we assessed the effects of isodrimenine derivatives across a range of acetylcholine (ACh) concentrations to distinguish competitive from noncompetitive inhibition, and we examined the voltage dependence of their action to determine whether the compounds act at luminal or nonluminal allosteric sites. Finally, using computational modeling, we proposed putative binding sites for the most potent compound, DH7KID, within the α7 nAChR structure.

2. RESULTS AND DISCUSSION

2.1. Chemical Characterization of Isodrimenine Derivatives. The structures of all synthesized compounds (Figure 2) were confirmed by elemental analysis, spectroscopy, and mass spectrometry (see section 2.3). Physicochemical constants of the reported compounds were consistent with previous studies.[12−14]

Bromination of drimenone **1** at positions C_{11} and C_{12} was confirmed by the presence of two AB systems in the ^{1}H NMR spectra, appearing as doublets at 4.12 and 4.27 ppm and 4.17 and 4.45 ppm (J = 9.7 Hz). This was further supported by the ^{13}C NMR spectrum of dibromide **3**, which showed characteristic signals at 23.23 and 23.72 ppm. In the infrared (IR) spectrum of compound **3**, absorption bands were observed at 692 cm^{-1} (−CH_2Br) and 1676 cm^{-1} (conjugated >C═O).

The IR spectrum of compound **4** exhibited absorption bands characteristic of −CH_2Br groups at 600 cm^{-1} and conjugated >C═C<C═O groups at 1649 and 1620 cm^{-1}, respectively. In the ^{1}H NMR spectrum of dibromide **4**, two AB systems were observed as doublets at 4.19 and 4.30 ppm and 4.41 and 4.57 ppm (J = 9.9 Hz), together with a singlet at 6.36 ppm corresponding to C_6−H. The ^{13}C NMR spectrum confirmed these assignments, showing signals for carbon atoms C_{11} (21.9 ppm), C_{12} (24.5 ppm), C_6 (123.9 ppm), and C_7 (177.6 ppm).

The presence of acetate groups in compounds **5** and **6** was supported by absorption maxima at 1236−1230 and 1743−1741 cm^{-1}, consistent with conjugated >C═C< (1632 cm^{-1}) and >C═O (1658−1677 cm^{-1}). In the ^{1}H NMR spectra, acetate groups were represented by singlets at 2.02−2.07 ppm and doublets at 4.68−5.05 ppm. Compound **6** also showed a C_6−H singlet at 6.31 ppm. The ^{13}C NMR spectra confirmed these findings, displaying signals at 20.8 and 26.1 ppm (OAc), 170.5−171.1 ppm (CH_3CO), and 124.0 ppm (C_6, compound **6**).

In the IR spectra of compounds **7** and **8**, characteristic hydroxyl adsorption bands were observed at 1065, 3321−3361, and 3310−3400 cm^{-1}, along with bands for conjugated >C═C−C═O groups at 1650−1658 cm^{-1}. The ^{1}H NMR spectra showed broad singlets for hydroxyl protons at 3.62−3.78 ppm and protons of methylene groups at C_{11} and C_{12} (4.32−4.65 ppm). The ^{13}C NMR spectra displayed signals at 56.1 ppm (C_{11}) and 58.0−58.5 ppm (C_{12}). The presence of a second double bond between C_5−C_6 was confirmed by a ^{13}C signal at 124.0 ppm and a corresponding C_6−H singlet at 6.31 ppm.

The structures of lactones **9** and **10** were confirmed by IR absorption bands at 1720−1783 cm^{-1} (α,β-unsaturated lactones) and 1683 cm^{-1} (conjugated >C═O). The ^{1}H NMR spectra of 7-keto-isodrimenine (**9**) and 5,6-dehydro-isodrimenine (**10**) each showed signals from a single methylene group at 4.81, 4.95, and 5.02 ppm, with corresponding ^{13}C signals for C_{12} at 67.2 and 67.4 ppm. Oxidation at C_{11} introduced two carbonyl signals (170.7 and 170.8 ppm). For compound **10**, the double bond between C_5−

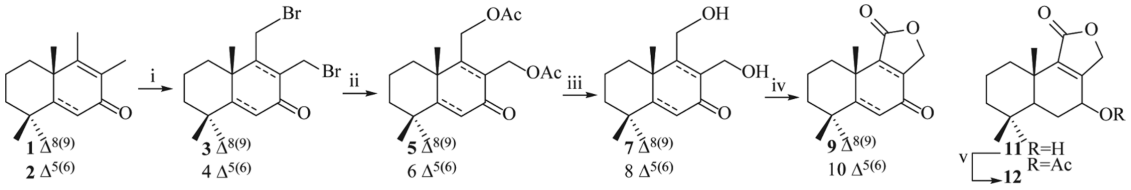

Figure 2. Scheme for the synthesis of isodrimenine derivatives. Compounds **9**, **10**, and **12** were derived from drimenone **1** and drimdienone **2**. (i) Compounds **1** and **2** were first brominated to compounds **3** and **4**, respectively. (ii) Treatment of bromides **3** and **4** with potassium acetate yielded acetates **5** and **6**. (iii) Saponification of compounds **5** and **6** produced diols **7** and **8**. (iv) Oxidation of diols **7** and **8** gave the target lactones 7-keto-isodrimenine (**9**; 7KID) and 5,6-dehydro-7-keto-isodrimenine (**10**; DH7KID), respectively. (v) 7-Acetoxy-isodrimenine (**12**; 7AID) was obtained by acetylation of 7-hydroxy-isodrimenine (**11**). Reagents and conditions: (i) NBS, CCl_4, reflux 3 h (for **1**) or 5 h (for **2**); (ii) KOAc, DMFA, RT, 2 h; (iii) K_2CO_3 (1%), MeOH, Ar, RT, 2 h; (iv) PCC, DCM, RT, 1.5 h; and (v) AcCl, DCM, DMA, RT, 22.5 h.

https://doi.org/10.1021/acschemneuro.5c00862
ACS Chem. Neurosci. 2026, 17, 260−274

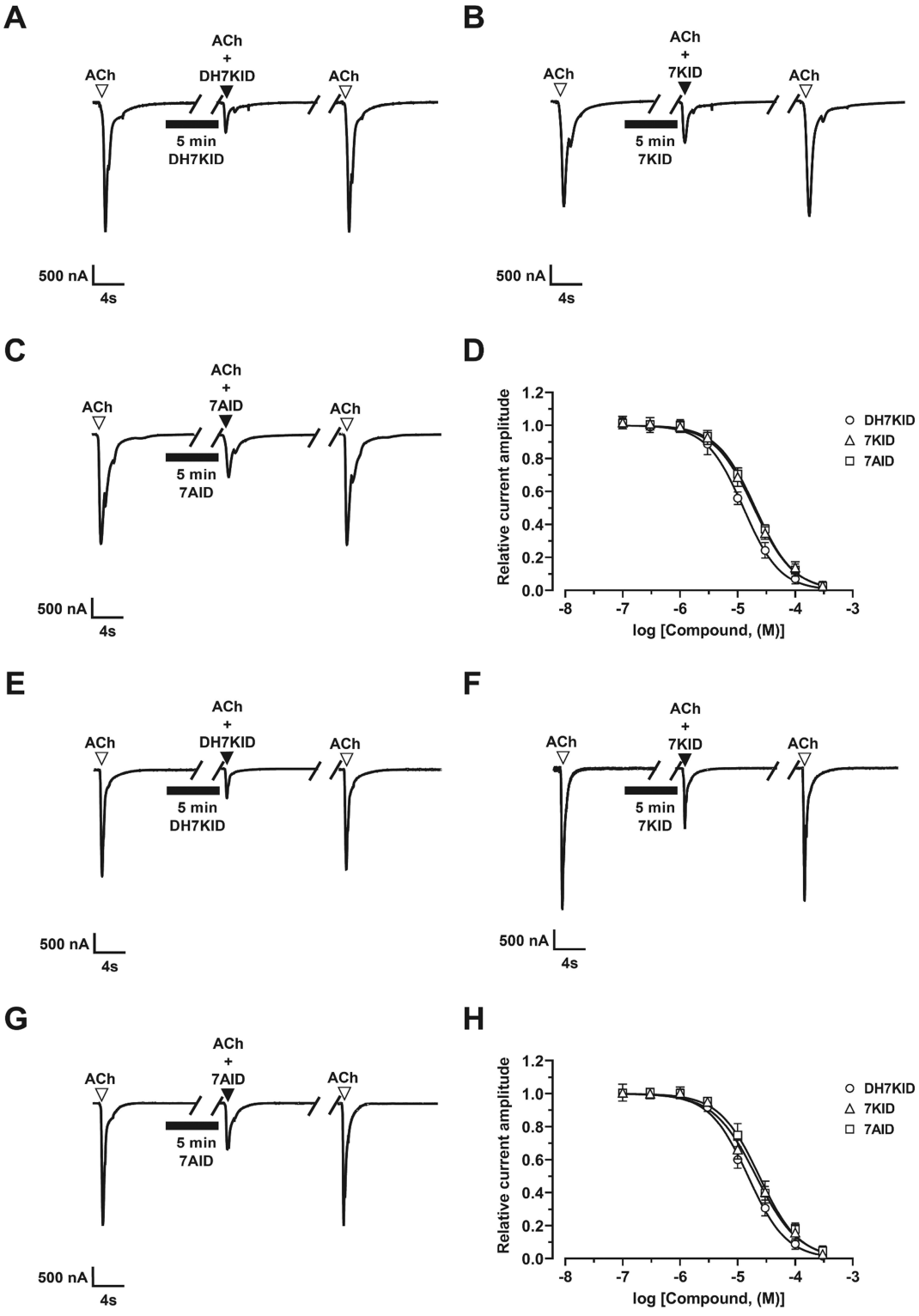

Figure 3. Effects of isodrimenine derivatives on human α7-containing nAChRs. Representative ACh (100 μM)-evoked nAChR currents recorded at − 80 mV in the presence of 30 μM DH7KID, 7KID, or 7AID at the $\alpha7\beta2$ (A-C) and $\alpha7$ (E-G) nAChR subtypes. (inverted triangle, open) ACh alone; (inverted triangle, closed) coapplication of ACh + compound after 5 min preincubation (full line, compound alone); (inverted triangle, open) ACh alone after washout. Concentration−response relationships (mean ± SD) for DH7KID (circle), 7KID (triangle), and 7AID (square) at the $\alpha7\beta2$ (n = 6−7) (D) and $\alpha7$ (n = 6−8) (H) subtypes. Calculated IC_{50}, n_H, and τ values are summarized in Table 1.

C_6 was confirmed by signals at 6.39 (^{1}H) and 124.8 ppm (^{13}C).

In compound **12**, the IR spectra showed absorption bands for acetate groups at 1736 and 1232 cm^{-1}, an α,β-unsaturated lactone at 1753 cm^{-1}, and a conjugated >C═O at 1736 cm^{-1}. The ^{1}H and ^{13}C NMR spectra of 7-acetoxy-isodrimenine (**12**) resembled those of 7-keto-isodrimenine (**9**), with an additional doublet of doublets at 5.56 ppm (C_7−H, 69.3 ppm). The acetate group was represented by a singlet at 2.11 ppm and ^{13}C signals at 21.1 and 171.2 ppm.

https://doi.org/10.1021/acschemneuro.5c00862
ACS Chem. Neurosci. 2026, 17, 260−274

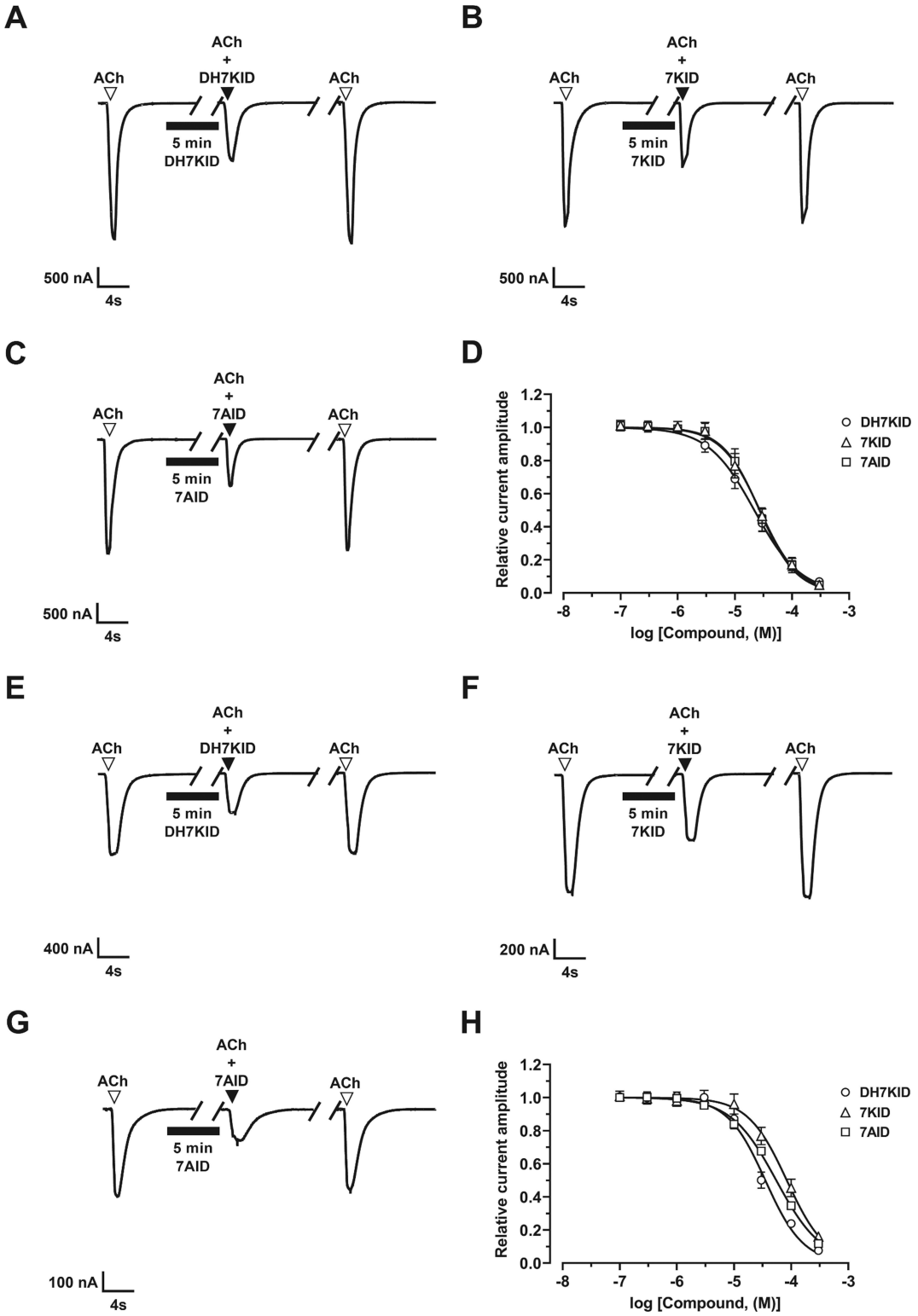

Figure 4. Effects of isodrimenine derivatives on human α4-containing nAChRs. (A−C) Representative ACh (6 μM ACh)-evoked currents recorded at −80 mV in the presence of 30 μM DH7KID, 7KID, or 7AID at the $\alpha4\beta4$ nAChR subtype. (E−G) Representative currents in the presence of 30 μM DH7KID, 100 μM 7KID, or 100 μM 7AID at the $\alpha4\beta2$ nAChR subtype (with 3 μM ACh). (inverted triangle, open) ACh alone; (inverted triangle, closed) coapplication of ACh + compound after 5 min preincubation (full line, compound alone); (inverted triangle, open) ACh alone after washout. Concentration−response relationships (mean ± SD) for DH7KID (circle), 7KID (triangle), and 7AID (square) at the $\alpha4\beta4$ (n = 10−14) (D) and $\alpha4\beta2$ (n = 7−8) (H) subtypes (with 3 μM ACh). Calculated IC_{50}, n_H, and τ values are summarized in Table 1.

2.2. Isodrimenine Derivatives Inhibit α7-Containing nAChRs More Potently than Other Subtypes. Isodrimenine derivatives neither activated nor potentiated but instead inhibited ACh-evoked currents mediated by human α7-, α4-, α3-, and α6*(*α6-α3 chimera)-containing nAChR subtypes, as well as the $\alpha9\alpha10$ nAChR (Figures 3−7). The chimeric $\alpha6/\alpha3$

https://doi.org/10.1021/acschemneuro.5c00862
ACS Chem. Neurosci. 2026, 17, 260−274

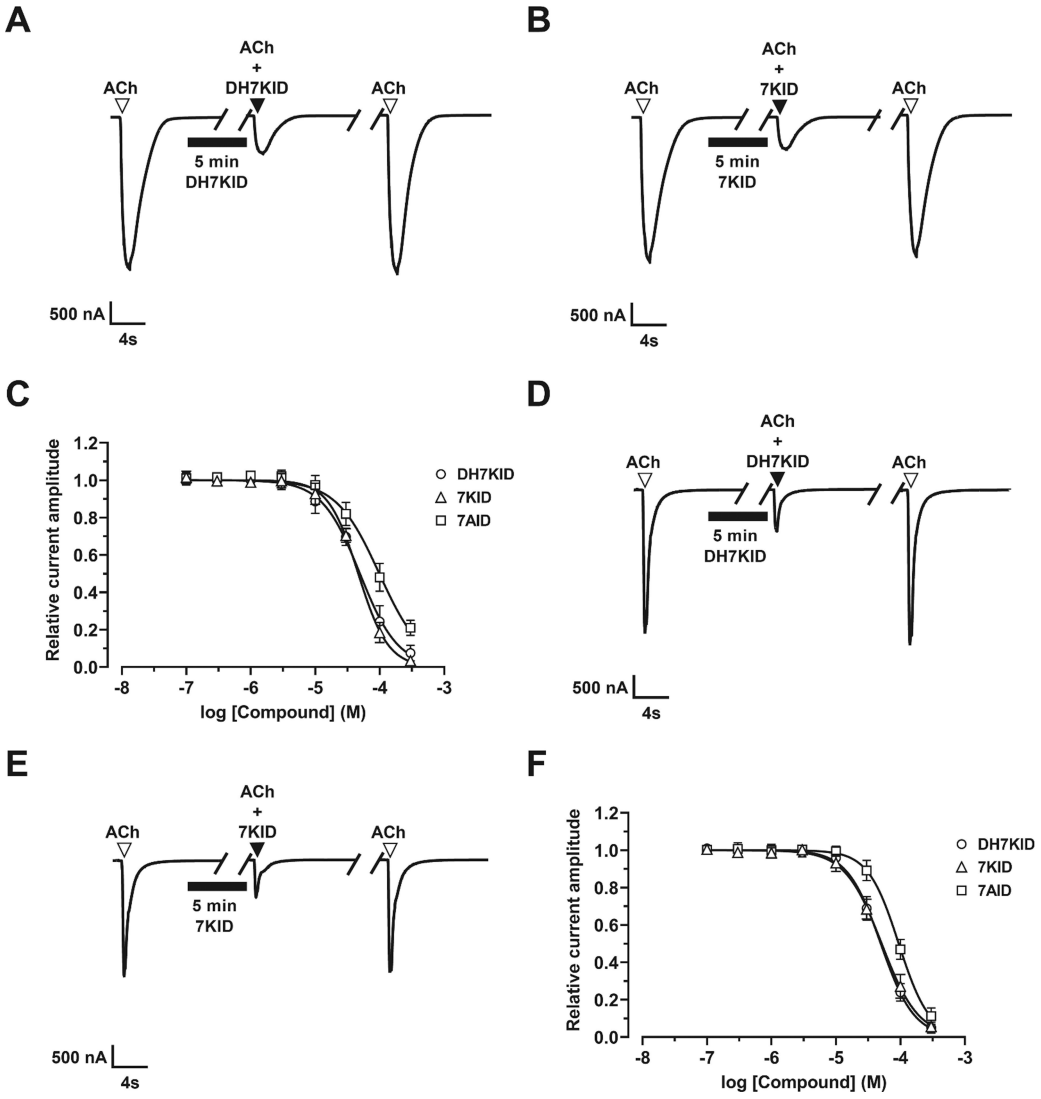

Figure 5. Effects of Isodrimenine Derivatives on human α3-containing nAChR subtypes. Representative ACh-evoked currents recorded at − 80 mV in the presence of 100 μM DH7KID or 7KID at the $\alpha3\beta4$ (with 300 μM ACh) (A, B) and $\alpha3\beta2$ (with 6 μM ACh) (D, E) nAChR subtypes. (inverted triangle, open) ACh alone; (inverted triangle, closed) coapplication of ACh + compound after 5 min preincubation (full line, compound alone); (inverted triangle, open) ACh alone after washout. Concentration−response relationships (mean ± SD) for DH7KID (circle), 7KID (triangle), and 7AID (square) at the $\alpha3\beta4$ (n = 7−9) (C) and $\alpha3\beta2$ (n = 7−10) (F) subtypes. Calculated IC_{50} and n_H values are summarized in Table 1.

subunit contained the extracellular domain of the α3 subunit in place of that of the α6.[15] Concentration−response relationships for the isodrimenine derivatives at each nAChR subtype (Figures 3D,H, 4D,H, 5C,F, 6C,F, and 7B) revealed the following selectivity profiles:

DH7KID: $\alpha7\beta2 \cong \alpha7 > \alpha4\beta4 > \alpha6^*\beta2\beta3 > \alpha4\beta2 \cong \alpha6^*\beta4 > \alpha3\beta4 \cong \alpha3\beta2 > \alpha9\alpha10$;

7KID: $\alpha7\beta2 \cong \alpha7 > \alpha4\beta4 > \alpha3\beta4 > \alpha3\beta2 \cong \alpha6^*\beta2\beta3 > \alpha6^*\beta4 > \alpha4\beta2 > \alpha9\alpha10$; and

7AID: $\alpha7\beta2 \cong \alpha7 > \alpha4\beta4 > \alpha6^*\beta2\beta3 > \alpha4\beta2 > \alpha6^*\beta4 > \alpha3\beta2 \cong \alpha3\beta4 \cong \alpha9\alpha10$.

Analysis of the calculated potencies (Table 1) showed that (1) all isodrimenine derivatives inhibited each nAChR subtype with similar potency; (2) the $\alpha7\beta2$ nAChR was inhibited more potently than other nAChR subtypes, whereas the $\alpha9\alpha10$ nAChR was least sensitive; (3) DH7KID (half-maximal inhibitory concentration (IC_{50}) = 22 μM), 7KID, and 7AID (IC_{50} = 27 μM) exhibited equivalent potency at $\alpha7\beta2$ nAChRs; (4) DH7KID, 7KID, and 7AID were equipotent at $\alpha4\beta4$ nAChRs; (5) 7KID inhibition of $\alpha4\beta4$ nAChRs 3-fold more strongly than $\alpha4\beta2$ nAChRs, suggesting a role for the $\beta4$ subunit. However, no similar selectivity was observed between $\alpha3\beta4$ and $\alpha3\beta2$ receptors, indicating that receptor sensitivity depends on specific α/β subunit interfaces; (6) DH7KID inhibited $\alpha6^*\beta2\beta3$ nAChRs with potency similar to $\alpha4\beta4$ nAChRs, whereas 7KID and 7AID were less potent, a trend also observed at $\alpha6^*\beta4$ nAChRs.

Hill coefficients for $\alpha7$- and $\alpha4$-containing nAChRs (n_H < 1.5) suggested noncooperative inhibition, whereas n_H > 1.5 at other subtypes indicated cooperative inhibition, with exceptions noted for $\alpha6^*\beta4$ (DH7KID) and $\alpha3\beta4$ and $\alpha6$-containing nAChRs (7AID) (Table 1).

2.3. Isodrimenine Derivatives Increase nAChR Desensitization. To determine whether isodrimenine-induced nAChR inhibition involved increased desensitization, we calculated the deactivation time constants (τ) for the most

https://doi.org/10.1021/acschemneuro.5c00862
ACS Chem. Neurosci. 2026, 17, 260−274

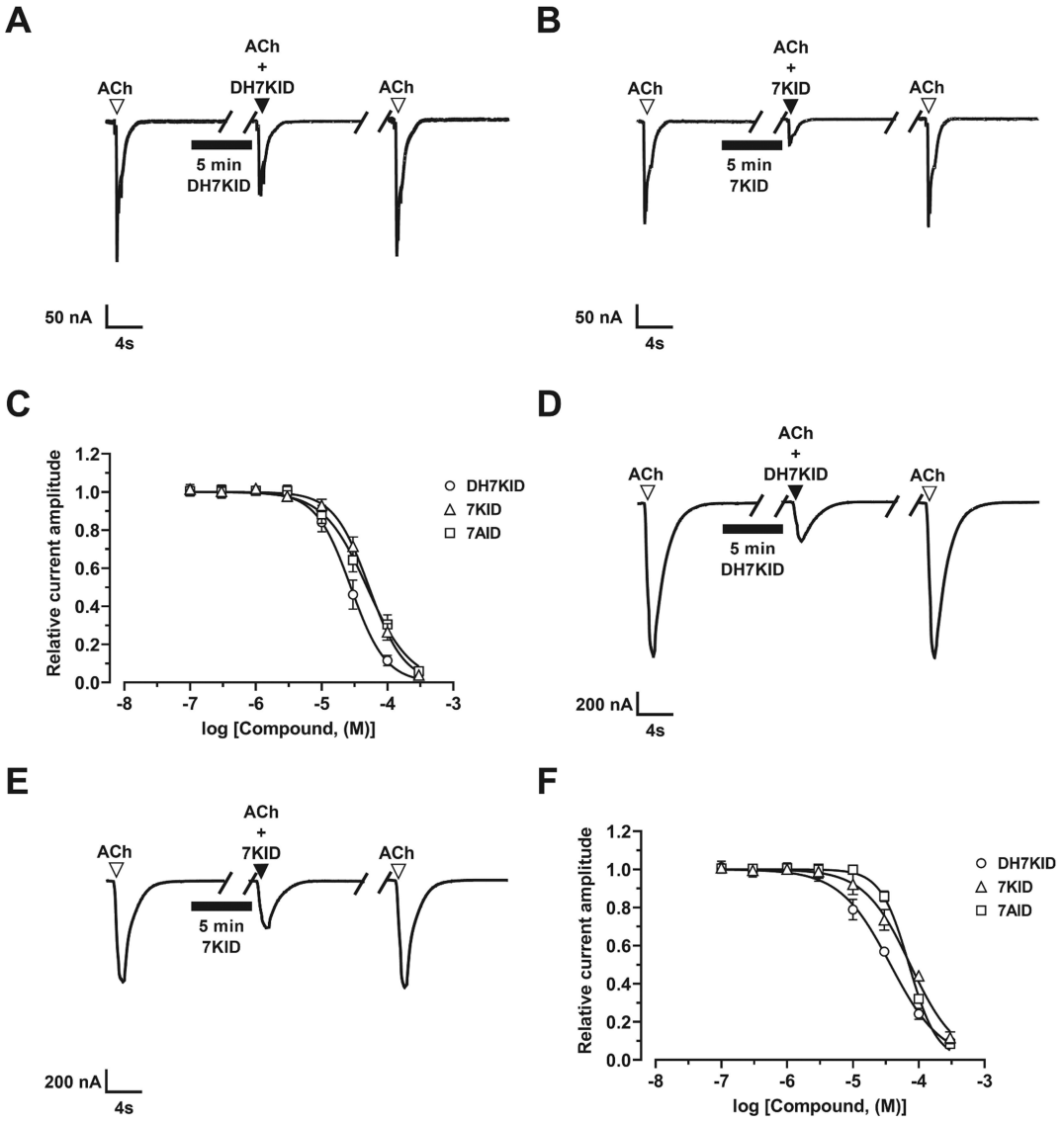

Figure 6. Effects of isodrimenine derivatives on α6-containing nAChR subtypes. (A, B) Representative ACh-evoked currents recorded at −80 mV in the presence of 30 μM DH7KID or 100 μM 7KID at the $\alpha6^*\beta2\beta3$ subtype (with 6 μM ACh). (D, E) Representative ACh-evoked currents in the presence of 100 μM DH7KID or 7KID at the $\alpha6^*\beta4$ subtype (200 μM ACh). (inverted triangle, open) ACh alone; (inverted triangle, closed) coapplication of ACh + compound after 5 min preincubation (full line, compound alone); (inverted triangle, open) ACh alone after washout. Concentration−response relationships (mean ± SD) for DH7KID (circle), 7KID (triangle), and 7AID (square) at the $\alpha6^*\beta2\beta3$ (n = 6−8) (C) and $\alpha6^*\beta4$ (n = 6) (F) subtypes. Calculated IC_{50} and n_H values are summarized in Table 1.

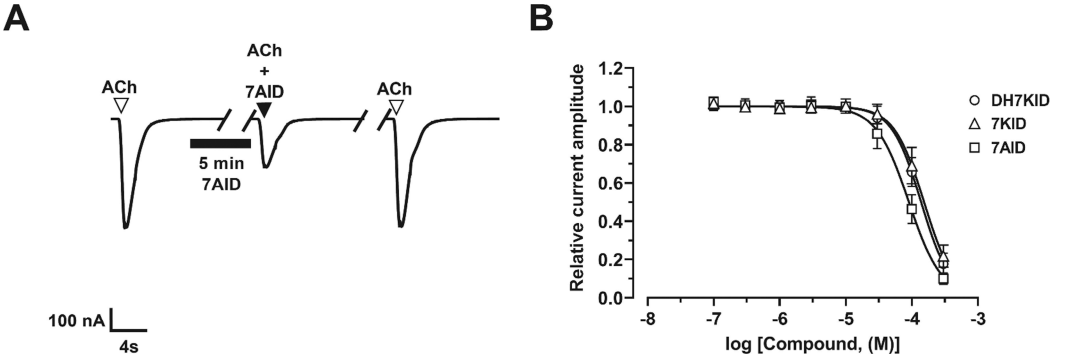

Figure 7. Effects of isodrimenine derivatives on the human $\alpha9\alpha10$ nAChR. (A) Representative ACh (6 μM)-evoked currents recorded at −80 mV in the presence of 100 μM 7AID. (inverted triangle, open) ACh alone; (inverted triangle, closed) coapplication of ACh + compound after 5 min preincubation (full line, compound alone); (inverted triangle, open) ACh alone after washout. (B) Concentration−response relationships (mean ± SD) for DH7KID (circle) 7KID (triangle), and 7AID (square). Calculated IC_{50} and n_H values are summarized in Table 1.

https://doi.org/10.1021/acschemneuro.5c00862
ACS Chem. Neurosci. 2026, 17, 260−274

Table 1. Pharmacological Activity of Isodrimenine Derivatives in Human nAChR Subtypes[c]

nAChR subtype	Isodrimenine derivative	IC_{50} (μM)	n_H	τ (s) ACh only[a]	τ (s) ACh[a] + isodrimenine derivative[b]
$\alpha7\beta2$	DH7KID	13 ± 1	1.4 ± 0.1	12.4 ± 0.1	12.3 ± 0.2
	7KID	19 ± 1	1.3 ± 0.1	12.4 ± 0.1	12.4 ± 0.1
	7AID	20 ± 1	1.3 ± 0.1	12.4 ± 0.1	12.4 ± 0.1
$\alpha7$	DH7KID	15 ± 1	1.3 ± 0.1	8.7 ± 0.2	8.6 ± 0.2
	7KID	21 ± 2	1.2 ± 0.1	8.7 ± 0.1	8.7 ± 0.1
	7AID	24 ± 2	1.3 ± 0.1	8.7 ± 0.1	8.6 ± 0.1
$\alpha4\beta4$	DH7KID	22 ± 1	1.1 ± 0.1	18.4 ± 0.1	18.4 ± 0.1
	7KID	27 ± 2	1.3 ± 0.1	18.5 ± 0.2	18.5 ± 0.2
	7AID	27 ± 2	1.1 ± 0.1	18.4 ± 0.1	18.4 ± 0.1
$\alpha4\beta2$	DH7KID	35 ± 3	1.3 ± 0.1	18.3 ± 0.2	18.3 ± 0.3
	7KID	84 ± 7	1.3 ± 0.1	18.1 ± 0.2	18.1 ± 0.3
	7AID	55 ± 4	1.1 ± 0.1	18.2 ± 0.3	18.2 ± 0.3
$\alpha3\beta4$	DH7KID	49 ± 4	1.5 ± 0.2		not determined
	7KID	46 ± 3	1.9 ± 0.2		
	7AID	99 ± 7	1.3 ± 0.1		
$\alpha3\beta2$	DH7KID	50 ± 3	1.7 ± 0.1		not determined
	7KID	51 ± 3	1.5 ± 0.2		
	7AID	94 ± 4	1.8 ± 0.2		
$\alpha6^*\beta2\beta3$	DH7KID	28 ± 2	1.6 ± 0.2		not determined
	7KID	53 ± 3	1.6 ± 0.2		
	7AID	49 ± 4	1.3 ± 0.1		
$\alpha6^*\beta4$	DH7KID	37 ± 3	1.1 ± 0.1		not determined
	7KID	74 ± 5	1.2 ± 0.2		
	7AID	71 ± 2	2.0 ± 0.2		
$\alpha9\alpha10$	DH7KID	138 ± 8	2.0 ± 0.2		not determined
	7KID	153 ± 10	1.5 ± 0.2		
	7AID	94 ± 4	1.9 ± 0.3		

[a]100 μM ACh at $\alpha7$ and $\alpha7\beta2$, 6 μM ACh at $\alpha4\beta4$ and 3 μM ACh at $\alpha4\beta2$ nAChRs. [b]30 μM at all subtypes except 100 μM 7KID and 7AID at $\alpha4\beta2$ nAChRs. [c]IC_{50} (half-maximal inhibitory concentration), n_H (Hill coefficient), and τ (deactivation time constant).

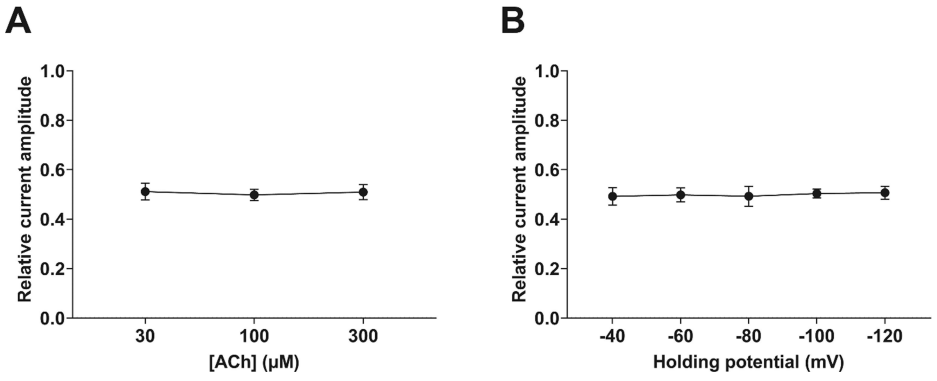

Figure 8. ACh concentration and membrane voltage dependence of DH7KID-induced $\alpha7$ nAChR inhibition. (A) Relative current amplitude for $\alpha7$ nAChR inhibition by 15 μM DH7KID (IC_{50} = 15 μM; see Table 1) at 30, 100, and 300 μM ACh. Student's test analysis (mean ± SD; n = 8) showed no significant difference among ACh concentrations ($p > 0.05$), supporting a noncompetitive inhibitory mechanism. Current amplitudes were normalized to responses elicited by the respective ACh concentration. (B) Voltage dependence of 15 μM DH7KID-induced $\alpha7$ nAChR inhibition using 100 μM ACh. Student's test analysis (mean ± SD; n = 6) showed no significant effect of membrane potential on DH7KID inhibition between − 40 mV and − 120 mV (compared to − 80 mV) ($p > 0.05$).

potent derivatives at the $\alpha7$- and $\alpha4$-containing nAChRs. The τ values of ACh-evoked currents at $\alpha7$, $\alpha7\beta2$, $\alpha4\beta2$, and $\alpha4\beta4$ receptors were unchanged in the presence of isodrimenines (Student's t test; $p > 0.05$; Table 1).

At h$\alpha7$ nAChRs, coapplication of 100 μM ACh with 30 μM DH7KID, 7KID, or 7AID resulted in τ values of 8.6−8.7 s, comparable to ACh alone. Similarly, τ values measured with 30 μM DH7KID, 7KID, or 7AID (12.3−12.4 s) were equivalent to ACh alone (12.4 s). At h$\alpha4\beta2$ nAChRs, τ values evoked by 3 μM ACh were unaffected by 30 μM DH7KID or 7AID or 100 μM 7KID (18.1−18.3 s vs ACh alone). Likewise, at $\alpha4\beta4$ nAChRs, τ values for 6 μM ACh (18.4−18.5s) were unchanged following exposure to 30 μM DH7KID, 7KID, or 7AID. Taken together, these results indicate that isodrimenine derivatives do not increase nAChR desensitization.

2.4. Isodrimenine Derivatives Inhibit $\alpha7$ and $\alpha4\beta4$ nAChRs via a Noncompetitive Mechanism. To determine whether inhibition involved the orthosteric site, we examined DH7KID (15 μM) and 7KID (30 μM) across varying ACh concentrations. DH7KID inhibition at $\alpha7$ nAChRs (relative

https://doi.org/10.1021/acschemneuro.5c00862
ACS Chem. Neurosci. 2026, 17, 260−274

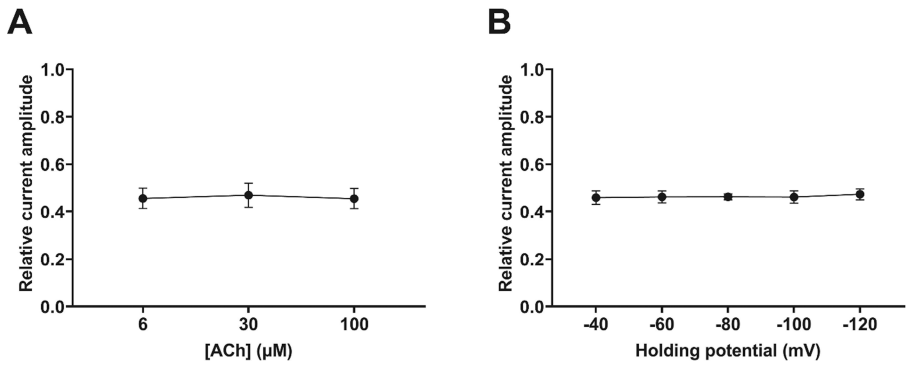

Figure 9. ACh concentration and membrane voltage dependence of 7KID-induced $\alpha4\beta4$ nAChR inhibition. (A) Relative current amplitudes for $\alpha4\beta4$ nAChR inhibition by 30 μM 7KID (near its IC_{50} = 27 μM; see Table 1) at 6, 30, and 100 μM ACh. Student's test analysis (mean ± SD; n = 10) showed no significant differences among ACh concentrations ($p > 0.05$), supporting a noncompetitive inhibitory mechanism. Current amplitudes were normalized to responses elicited by the respective ACh concentration. (B) Voltage dependence of 30 μM 7KID-induced $\alpha4\beta4$ inhibition using 6 μM ACh. Student's test analysis (mean ± SD; n = 7) showed no significant effect of membrane potential on 7KID inhibition between −40 and − 120 mV (compared with −80 mV) ($p > 0.05$).

current amplitude at 100 μM ACh = 0.51 ± 0.03) was unchanged at 30 μM (0.51 ± 0.03) or 300 μM ACh (0.52 ± 0.03, n = 8; $p > 0.05$; Figure 8A). Similarly, 7KID at $\alpha4\beta4$ nAChRs (relative current amplitude at 6 μM ACh = 0.46 ± 0.04) was unaffected by 30 μM ACh (0.47 ± 0.05) or 100 μM ACh (0.46 ± 0.04, n = 10; $p > 0.05$; Figure 9A). These findings indicate that isodrimenine derivatives inhibit nAChRs via a noncompetitive mechanism independent of the orthosteric binding site.

2.5. Inhibitory Activity of Isodrimenines at $\alpha7$ and $\alpha4\beta4$ nAChRs Is Voltage-Independent. To further characterize the inhibitory mechanism, we assessed DH7KID and 7KID at $\alpha7$ or $\alpha4\beta4$ nAChRs across membrane potentials from −40 to − 120 mV (in − 20 mV increments). Inhibition by 15 μM DH7KID on $\alpha7$-mediated currents (100 μM ACh; n = 6; Figure 8B) and 30 μM 7KID on $\alpha4\beta4$-mediated currents (6 μM ACh; n = 7; Figure 9B) did not vary significantly with voltage compared to −80 mV. This voltage-independent inhibition is consistent with nonluminal binding site(s). Together, these results (Sections 2.3, 2.4, and 2.5) support a mechanism of negative allosteric modulation.

2.6. Putative Docking Sites for DH7KID Docking Sites Are Located at Nonluminal Allosteric Regions of the $\alpha7$ nAChR. Molecular docking simulations of the $\alpha7$ nAChR model identified 22 distinct nonhomologous docking sites and generated 682 conformers. Using the MM-GBSA method, one conformer per site was selected based on theoretical binding energy (TBE) values, and 300 ns MD simulations assessed stability. Four stable conformers were identified, defining four putative docking sites: the extracellular-transmembrane (ECD-TMD), transmembrane (TMD), cytoplasmic (CYD), and TMD-CYD sites (Figure 10A; Table 2). All sites were located at intersubunit interfaces. Although $\alpha7$ nAChR consists of five identical subunits, its pentameric arrangement is asymmetrical, resulting in structural variations among the interfaces. For clarity, $\alpha7$ subunits were designated $\alpha7$a—$\alpha7$e anticlockwise from the extracellular view. Conformers were considered stable if the root-mean-square deviation (RMSD) variance remained below 0.5.

The putative ECD-TMD site is located at the ECD-TMD junction at the $\alpha7$c(+)/$\alpha7$d(—) interface, facing the pore (ECD vestibule and TMD ion-channel). DH7KID binding at this site (TBE = −4.4 ± 0.8 kcal/mol; RMSD = 8.2) was predominantly through weak π−alkyl or hydrophobic interactions (Figure 10C; Table 2). The relatively large RMSD value reflects the movement of this conformer from its initial docking position, located slightly toward the ECD, to its final, more stable orientation, as indicated by an RMSD variance of 0.2 (Figure 10B; Table 2). Interacting residues from the $\alpha7$c(+) subunit included A280 and E281 (TM2), while residues from the $\alpha7$d(—) subunit included Y232, Y233, N236, and L237 (TM1), L278 and E281 (TM2), and I282 (TM2-TM3 Loop).

The putative TMD site is located at the $\alpha7$a(+)/$\alpha7$b(—) subunit interface near the TMD-CYD junction. DH7KID interactions at this site (TBE = −9.5 ± 2.7 kcal/mol; RMSD = 5.3) were predominantly hydrophobic or weak π−alkyl (Figure 10D; Table 2). The RMSD reflects a rotation of the conformer from its initial docking position, after which it remained stable through the rest of the MD simulation, as shown by a low variance of 0.2 (Figure 10B; Table 2). Interacting residues from the $\alpha7$a(+) subunit included L269, T273, M276, L277, A280 (TM2), and M301 (TM3), whereas the $\alpha7$b(—) subunit contributed L235, N236, P240, and L243 (TM1) and S271, F275, and L278 (TM3).

The putative TMD-CYD site is positioned at the $\alpha7$d(+)/$\alpha7$e(—) interface in contact with the membrane. DH7KID interactions at this site (TBE = −5.9 ± 1.3 kcal/mol; RMSD = 5.6) involved one hydrogen bond with $\alpha7$e-R469, with the remaining interactions being hydrophobic or weak π−alkyl (Figure 10E; Table 2). The mean RMSD also corresponds to rotational movements, as the conformer remained near the original docking site. This site exhibited the lowest variance (0.2) of all, confirming its stability. Within the $\alpha7$d(+) interface, DH7KID interacted with R316 and Y317 (TM3) and H320 and D321 (TM3-MX Loop), whereas in the $\alpha7$e(—) interface, it also interacted with M345 and R347 (MX-TM4 Loop), F462 and C465 (MA helix), and R469 (TM4).

The putative CYD site is composed of five MX helices, one from each of the five subunits, located at the base of the cytoplasmic vestibule. Figure 10B shows the RMSD plots for each site, starting at 50 ns, when the conformers stabilized from their initial docking positions. This site is narrow and symmetrical, surrounded by conserved residues across subunits. DH7KID rotated during MD yet remained in

https://doi.org/10.1021/acschemneuro.5c00862
ACS Chem. Neurosci. 2026, 17, 260−274

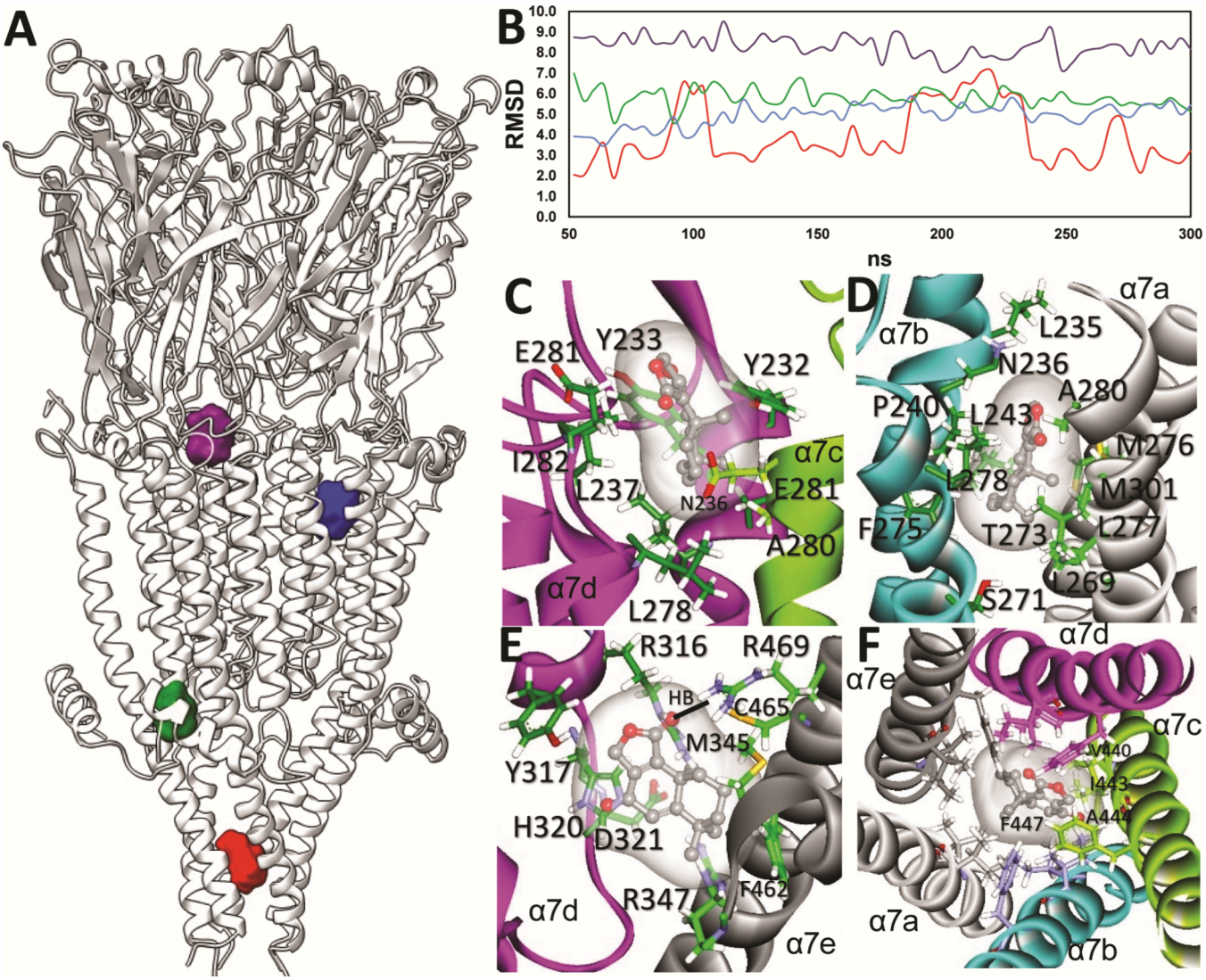

Figure 10. Molecular docking and molecular dynamics simulations of DH7KID at the α7 nAChR model. (A) Overview of the α7 nAChR model showing DH7KID docking sites (molecular surfaces), including the ECD-TMD (purple), TMD (blue), TMD-CYD (green), and CYD (red) regions. (B) RMSD plots from 300 ns MD simulations of DH7KID at each docking site (color codes as in A). (C) Molecular details of the ECD-TMD site at the α7c(+)(green)/α7d(—)(magenta) interface, showing weak π–alkyl [Y232, L237 (TM1), A280 (TM2)] and hydrophobic [Y233, N236 (TM1), L278, E281, I282 (TM2)] interactions with DH7KID. (D) Molecular details of the TMD site at the α7a(+)(white)/α7b(—)(cyan) interface, showing π–alkyl [P240, L243 (TM1), F275, M276 (TM2), M301 (TM3)] and hydrophobic [L235, N236 (TM1), L269, S271, T273, L277, L278, and A280 (TM2)] interactions. (E) Molecular details of the TMD-CYD site at the α7d(+)(magenta)/α7e(—)(gray) interface, showing π–alkyl [H320 (TM3-MX Loop), M345, R347 (MX-TM4 Loop), F462, C465 (MA helix), hydrophobic [R316, Y317 (TM3), D321 (TM3-MX Loop)], and hydrogen bond [R469 (TM4)] (---) interactions. (F) Molecular details of the CYD site at the interface of the five subunits. Residues from the MA helix (V440, I443, A444, and F447) are conserved across all subunits, mediating hydrophobic or π–alkyl interactions. (C–F) DH7KID is shown as a ball-and-stick representation (hydrogens omitted for clarity), while α7 residues are shown in stick representation. Atom coloring: C green/gray; O red; N blue; H white.

position, forming hydrophobic and weak π–alkyl contacts with identical residues (V440, I443, A444, and F447) in each subunit.

The superior potency of DH7KID compared with 7KID and 7AID can be attributed to its unique structural and physicochemical features. The C_7 carbonyl group in DH7KID and 7KID and the acetate in 7AID serve as hydrogen bond acceptors, stabilizing interactions such as the R469 hydrogen bond at the TMD–CYD interface. The planar α,α'-dienone system in DH7KID increases the π-surface area, enhancing hydrophobic π–alkyl contacts. Its moderate lipophilicity promotes partitioning into the membrane, facilitating access to lipid-adjacent sites at the TMD and TMD-CYD interfaces. Although ranked third by TBE, the TMD-CYD site showed the greatest binding stability, suggesting that DH7KID combines optimal physicochemical properties with a specific hydrogen bonding capability to efficiently target membrane-adjacent allosteric sites via lateral diffusion.

2.7. Molecular Properties of the Isodrimenine Derivatives. DH7KID exhibited physicochemical properties favoring partitioning into lipid bilayers: QPlogPo/w = 2.7, polar surface area (PSA) = 43.4 Å^2, fraction of hydrophobic surface (Fh) = 0.69, π contribution of SASA (PISA) = 17.6 Å^2, and QPPCaco = 665 nm/s (Table 3). These values indicate moderate lipophilicity, low polarity, a high fraction of hydrophobic surface, and a high predicted passive permeability.

https://doi.org/10.1021/acschemneuro.5c00862
ACS Chem. Neurosci. 2026, 17, 260–274

Table 2. Docking Sites for DH7KID in the Human α7 nAChR Model[a]

Site	TBE Mean ± SE	RMSD Mean + SE	RMSD Mean (variance)	Involved residues
ECD-TMD	−4.4 ± 0.8	−3.6	8.2 (0.2)	**α7d** TM1: Y232 (π), Y233 (H), N236 (H), L237 (π) TM2: L278 (H), E281 (H) M2-M3 Loop: I282 (H) **α7c** TM2: A280 (π), E281 (H)
TMD	−9.5 ± 2.7	−6.8	5.3 (0.2)	**α7b** TM1: L235 (H), N236 (H), P240 (π), L243 (π) TM2: S271 (H), F275 (π), L278 (H) **α7a** TM2: L269 (H), T273 (H), M276 (π), L277 (H), A280 (H) TM3: M301 (π)
TMD-CYD	−5.9 ± 1.3	−4.6	5.6 (0.1)	**α7d** TM3: R316 (H), Y317 (H) TM3-MX Loop: H320 (π), D321(H) **α7e** MX-TM4 Loop: M345 (π), R347 (π) MA: F462 (π), C465 (π) TM4: R469 (HB)
CYD	−15 ± 2.1	−13	3.2 (0.3)	**α7a** MA: V440 (H), I443 (π), F447 (π) **α7b** MA: V440 (π), I443 (H), F447 (H) **α7c** MA: V440 (π), I443 (H), A444 (H), F447 (H) **α7d** and **α7e** MA: V440 (H), I443 (π), F447 (H)

[a]Mean ± SE (standard error) and mean (variance) values were obtained from the last 100 ns of the MD simulations. Mean + SE, negative upper limits reflect stable conformations. Most residues interact with DH7KID through π−alkyl (π) or hydrophobic (H) contacts, except α7e-R469, which forms a hydrogen bond (HB). TM1−TM4: transmembrane segments. MA, MX: cytoplasmic helices.

Table 3. Molecular Properties of the Isodrimenine Derivatives

Molecular properties	DH7KID	7KID	7AID
LogP	2.7	2.529	2.807
PSA (Å^2)	67.8	67.6	73.2
SASA (Å^2)	464	438.9	529.5
FOSA (Å^2)	322.9	341.6	435.2
FISA (Å^2)	123.7	94.7	91.6
PISA (Å^2)	17.631	2.681	2.695
Fh = FOSA/(FOSA+FISA)	0.72	0.78	0.83
QPPCaco (nm/s)	664.6	1253.4	1339.4
QPPMDCK (nm/s)	318.1	631.5	678.5
QPlogS	−2.40	−1.92	−3.47
human oral absorption (%)	85.3	90.7	100

Across all putative docking sites (i.e., ECD-TMD, TMD, TMD-CYD, and CYD), DH7KID formed extensive hydrophobic and π−alkyl interactions. At the TMD-CYD interface, a hydrogen bond between the C_7 carbonyl of DH7KID and R469 provided additional polar stabilization. Together, these features explain the prevalence of π−alkyl interactions and the preferential targeting of membrane-adjacent binding sites by DH7KID.

2.8. Isodrimenine Derivatives Act as Negative Allosteric Modulators of the α7 nAChR. Our results provide strong evidence that isodrimenine derivatives inhibit α7 nAChRs through interactions with putative binding sites located at nonluminal allosteric regions. This conclusion was supported by several functional and structural observations: (1) the inhibitory activity of DH7KID at α7 nAChRs and of 7KID at α4β4 nAChRs was largely unchanged across different ACh concentrations, indicating that isodrimenine derivatives do not interact with the orthosteric site; (2) the inhibition of both α7 and α4β4 nAChRs by these compounds was unaffected by variations in membrane potential, suggesting that they do not act by directly blocking the ion-channel lumen; and (3) molecular docking and MD simulations revealed that DH7KID interacts with multiple putative allosteric sites on the α7 nAChR. Although these computational results are not definitive,[16] they provide a valuable framework for future site-directed mutagenesis studies. Taken together, these findings support a mechanism in which isodrimenine derivatives function as negative allosteric modulators of α7 nAChRs.

2.9. Comparison between Isodrimenine Derivatives and Drimane Sesquiterpenoids. Comparative analysis with previously studied drimane sesquiterpenoids[6] highlights several key distinctions: (i) isodrimenine derivatives inhibit α7 nAChRs more potently than α4β2 nAChRs, whereas drimane sesquiterpenoids show the opposite trend; (ii) isodrimenine derivatives interact with four intersubunit sites on the α7 nAChR, whereas drimane sesquiterpenoids target β2 intrasubunit and luminal sites; (iii) isodrimenine derivatives primarily interact with TM1 and TM2 residues, whereas drimane sesquiterpenoids bind to TM3 and TM4; and (iv) drimane sesquiterpenoids form multiple hydrogen bonds with the lactone oxygens, whereas isodrimenines form a single hydrogen bond with R469 at the TMD−CYD interface.

3. CONCLUSIONS

α7-containing nAChRs are widely distributed throughout the central and peripheral nervous systems, as well as in immune cells, where they regulate key physiological functions.[17] Activation of α7 receptors promotes neurotransmitter release, neuroprotection, cognitive enhancement, and anti-inflammatory effects, with therapeutic relevance to Alzheimer's disease, Parkinson's disease, schizophrenia, and mood disorders.[18] Given the high oral bioavailability of isodrimenines, their ability to inhibit α7-containing nAChRs suggests potential therapeutic applications under various neurological and neuropsychiatric conditions. This is especially relevant considering that selective antagonists like MLA, as well as negative allosteric modulators (α7-NAMs) such as SB-277011 and BNC210, have demonstrated pro-cognitive, anti-inflammatory, antidepressant, and anxiolytic-like activity in rodent models.[7−11,19,20]

Overall, isodrimenine derivatives act as negative allosteric modulators, inhibiting α7 nAChRs more potently than other

https://doi.org/10.1021/acschemneuro.5c00862
ACS Chem. Neurosci. 2026, 17, 260−274

nAChR subtypes. Their binding occurs at multiple putative intersubunit sites, primarily adjacent to the lipid bilayer at the TMD and TMD−CYD interfaces. The selectivity and stability of $\alpha 7$ receptor inhibition by isodrimenines may hold clinical significance for the development of novel therapeutics targeting neuropsychiatric disorders.

4. METHODS

4.1. Materials. Acetylcholine chloride, 1,2-bis(2-aminophenoxy)-ethane-*N*,*N*,*N*′,*N*′-tetraacetic acid tetrakis acetoxymethyl ester (BAPTA-AM), ethyl 3-aminobenzoate methanesulfonate, collagenase A, *N*-bromosuccinimide (NBS), bovine serum albumin (BSA), and all analytical-grade as salts and solvents used for the synthesis of isodrimenines and intermediates were purchased from Sigma-Aldrich (St. Louis, MO, USA). Thin-layer chromatography (TLC) silica gel 60 plates were obtained from Merck (Rahway, NJ, USA). Fetal bovine serum (FBS) was obtained from Bovogen (East Keilor, VIC, Australia). Gentamicin and penicillin-streptomycin were purchased from Invitrogen Life Technologies (Carlsbad, CA, USA).

4.2. Synthesis of Isodrimenine Derivatives. The synthesis of the reported isodrimenine derivatives (Figure 2) (see Figure 1 for structures) was based on the sesquiterpene intermediates drimenone **1** and drimdienone **2**, both derived from the natural labdane diol (+)-sclareol.[21] Bromination with variable amounts of NBS yielded bromides **3** and **4** in 99% and 76% yields, respectively. For the synthesis of 11,12-dibromodrim-8(9)-en-7-one (**3**), drimenone **1** (1 mmol) was dissolved in dry carbon tetrachloride (CCl_4, 15 mL), and 2 mmol of NBS was added. The mixture was refluxed for 3 h and then eluted with a mixture of petroleum ether (EP)/diethyl ether (Et_2O) (9.5:0.5). 11,12-Dibromodrim-5,8(9)-dien-7-one (**4**) was prepared from drimdienone **2** using 1.8 mmol of NBS under reflux for 5 h and eluted with PE/Et_2O (4:1).

After cooling, each reaction mixture was filtered, solvents were removed, and the crude reaction product was purified by silica gel column chromatography. Treatment of bromides **3** and **4** with potassium acetate (KOAc) under standard conditions afforded acetates **5** and **6** in yields of 77% and 95%, respectively. Specifically, KOAc (2 mmol) was added to a solution of dibromide **3** or **4** (1 mmol) in *N*,*N*-dimethylformamide (DMFA, 7 mL). The reaction mixture was stirred at room temperature (RT) for 2 h, diluted with H_2O (20 mL), and extracted with Et_2O (3 × 15 mL). The combined organic layers were washed with H_2O (3 × 10 mL), dried over anhydrous Na_2SO_4, and concentrated *in vacuo*.

Purification by silica gel column chromatography yielded 11,12-diacetoxydrim-8(9)-en-7-one (**5**), eluted with PE/Et_2O (9.5:0.5), and 11,12-diacetoxydrim-5,8(9)-dien-7-one (**6**) eluted with PE/Et_2O (95:5), both obtained as colorless oils. Compounds **5** and **6** were separately subjected to saponification into diols **7** and **8**, respectively, in yields of 72 and 70%, respectively. Briefly, a solution of 1% K_2CO_3 in MeOH (14 mL) was added to a solution of diacetate **5** or **6** (1 mmol) in MeOH (4 mL), and the mixture was stirred under Ar at RT for 2 h, diluted with H_2O (100 mL), and extracted with Et_2O (3 × 30 mL). The combined organic layers were washed sequentially with a 10% H_2SO_4 solution (10 mL) and water (3 × 30 mL) and then dried over anhydrous Na_2SO_4. After removal of the solvent under reduced pressure, the crude products were purified by silica gel column chromatography. 11,12-Dihydroxydrim-8(9)-en-7-one (**7**) was eluted with PE/Et_2O (4:6), while 11,12-dihydroxydrim-5,8(9)-dien-7-one (**8**) was eluted with PE/Et_2O (6:4).

Target lactones 7-keto-isodrimenine **9** (7KID) and 5,6-dehydro-7-keto-isodrimenine **10** (DH7KID) were obtained in 92 and 82% yields, respectively, by the oxidation of diols **7** and **8** with pyridinium chlorochromate (PCC) under the conditions shown. PCC (5 mmol) was added to a solution of diol **7** or **8** (1 mmol) in dichloromethane (DCM, 7 mL), and the mixture was stirred at RT for 1.5 h. The reaction mixture was filtered through a silica gel bed with Et_2O, and after solvent removal, the crude product was purified by silica gel column chromatography. Both 7KID and DH7KID were eluted separately with PE/Et_2O (9:1). The third target compound, 7-acetoxy-isodrimenine (**12**) (7AID), was synthesized by the acetylation of 7-hydroxy-isodrimenine (**11**) in 90% yield. Briefly, *N*,*N*-dimethylaniline (0.1 mmol) was added to a solution of 1 mmol of 7-hydroxy-isodrimenine (**11**) in DCM (8 mL), and the mixture was stirred for 30 min at RT, before acetyl chloride (1 mmol) was added. The reaction was stirred for 22 h at RT, diluted with H_2O (20 mL), and extracted with Et_2O (3 × 15 mL). The combined organic layers were washed with H_2O (3 × 10 mL), dried over anhydrous Na_2SO_4, and concentrated *in vacuo*. The crude product was purified by silica gel column chromatography, and 7AID was eluted with PE/Et_2O (9.5:0.5).

4.3. Chemical Characterization. Infrared spectra were recorded on a Spectrum 100 FT-IR spectrometer (PerkinElmer, Shelton, CT, USA) using the attenuated total reflectance (ATR) technique. ^1H and ^{13}C NMR spectra (400 and 100 MHz, respectively) were acquired on a Bruker Avance DRX 400 spectrometer (Bruker BioSpin, Rheinstetten, Germany) in $CDCl_3$. ^1H NMR chemical shifts are reported relative to residual solvent protons (7.26 ppm) as internal standards, while solvent carbon atoms (77.0 ppm) served as an internal standard for the ^{13}C NMR spectra. Optical rotation measurements were performed on a Jasco DIP-370 polarimeter (Rudolph Research Analytical, Hackettstown, NJ, USA) using a 10 cm microcell. Melting points were determined with a Boethius hot stage apparatus (VEB Analytik, Dresden, Germany) and are not uncorrected. Reaction progress and product purity were monitored by TLC on silica gel 60 plates using mixtures of EP/Et_2O as eluents. Visualization was achieved by treatment with concentrated H_2SO_4 followed by heating at 80 °C or UV lamp irradiation (254 or 365 nm). All solvents were purified and dried by standard methods before use.

*11,12-Dibromodrim-8(9)-en-7-one (**3**) (99% Yield as White Crystals).* Mp 107−108 °C (from PE), $[\alpha]_D^{20}$ = +30.5° (*c* 6.2). Found (%): C, 47.42; H, 5.43; O, 5.06; Br, 42.09. $C_{15}H_{22}OBr_2$. Calculated (%): C, 47.64; H, 5.86; O, 4.24; Br, 42.26. IR spectra (ATR, ν/cm^{-1}): 2928, 2850, 1676, 1462, 1333, 1204, 692. ^1H NMR ($CDCl_3$): δ 0.91 (s, 3H, 13-H_3), 0.94 (s, 3H, 14-H_3), 1.18 (s, 3H, 10-H_3), 1.78 (dd, 1H, *J* = 3.4, 14.3 Hz, 5-*H*), 2.44 (dd, 1H, *J* = 14.2, 17.4 Hz, 6-*H*) and 2.61 (dd, 1H, *J* = 3.7, 17.4 Hz, 6-*H*), 4.12 and 4.27 (both d, AB spin system, 2H, *J* = 9.7 Hz, 11-H_2), 4.17 and 4.45 (both d, AB spin system, 2H, *J* = 9.7 Hz, 12-H_2). ^{13}C NMR ($CDCl_3$): δ 18.4 (C_2), 18.5 (C_{15}), 21.3 (C_{13}), 23.23 (C_{11}), 23.72 (C_{12}), 32.4 (C_{14}), 33.3 (C_4), 35.1 (C_6), 35.2 (C_1), 40.6 (C_3), 41.2 (C_{10}), 49.8 (C_5), 134.9 (C_9), 165.4 (C_8), 196.8 (C_7). 11,12-*Dibromodrim-5,8(9)-dien-7-one* (**4**) (76% yield as white crystals): mp 136−137 °C (from PE), $[\alpha]_D^{20}$ +23.9 ° (*c* 3.4). Found (%): C, 48.05; H, 5.40; O, 4.30; Br, 42.25. $C_{15}H_{20}OBr_2$. Calculated (%): C, 47.81; H, 5.35; O, 4.36; Br, 42.48. IR spectra (ATR, ν/cm^{-1}): 3046, 2923, 2868, 1770, 1685, 1649, 1620, 1428, 1373, 1187, 820. ^1H NMR ($CDCl_3$): δ 1.21 (s, 3H, 13-H_3), 1.29 (s, 3H, 14-H_3), 1.40 (s, 3H, 15-H_3), 4.19 and 4.30 (both d, AB spin system, 2H, *J* = 10.3 Hz, 11-H_2), 4.41 and 4.57 (both d, AB spin system, 2H, 2H, *J* = 9.9 Hz, 12-H_2). 6.36 (s, 1H, 6-*H*). ^{13}C NMR ($CDCl_3$): δ 18.0 (C_2), 25.8 (C_{15}), 28.8 (C_{13}), 21.9 (C_{11}), 24.5 (C_{12}), 32.4 (C_{14}), 37.5 (C_4), 34.9 (C_1), 40.6 (C_3), 44.5 (C_{10}), 123.9 (C_6), 135.4 (C_9), 161.2 (C_8), 177.6 (C_5), 183.8 (C_7).

*11,12-Diacetoxydrim-8(9)-en-7-one (**5**) (77% Yield as Colorless Oil).* $[\alpha]_D^{20}$ = +42.6° (*c* 1.2). Found (%): C, 67.56; H, 8.29; and O, 24.15. $C_{19}H_{28}O_5$. Calculated (%):C, 67.83; H, 8.38; O, 23.79. IR spectra (ATR, ν/cm^{-1}): 2991, 2872, 1743, 1677, 1381, 1236, 1141, 1029. ^1H NMR ($CDCl_3$): δ 0.91 (s, 3H, 13-H_3), 0.94 (s, 3H, 14-H_3), 1.18 (s, 3H, 15-H_3), 1.79 (dd, 1H, *J* = 3.6, 14.2 Hz, 5-*H*), 2.02 (s, 3H, OAc), 2.07 (s, 3H, OAc), 2.44 (dd, 1H, *J* = 14.2, 17.0 Hz, 6-*H*) and 2.59 (dd, 1H, *J* = 3.4, 17.7 Hz, 6-*H*), 4.85 (d, 2H, *J* = 2.4 Hz, 11-H_2), 4.68 (d, 1H, *J* = 11.7 Hz, 12-*H*) and 4.87 (d, 1H, *J* = 12.3 Hz, 12-*H*). ^{13}C NMR ($CDCl_3$): δ 18.3 (C_{15}), 18.4 (C_2), 20.8 (both OAc), 21.2 (C_{13}), 32.4 (C_{14}), 33.1 (C_4), 34.8 (C_1), 35.2 (C_6), 40.4 (C_{10}), 40.9 (C_3), 49.7 (C_5), 57.2 (C_{11}), 57.4 (C_{12}), 134.9 (C_9), 165.4 (C_8), 170.1 and 170.5 (both $CH_3\underline{CO}$), 196.8 (C_7).

*11,12-Diacetoxydrim-5,8(9)-dien-7-one (**6**) (95% Yield as Colorless Oil).* $[\alpha]_D^{23}$ = +32.9° (*c* 0.34). Found (%): C, 68.25; H, 8.04; O, 23.71. $C_{19}H_{26}O_5$. Calculated (%): C, 68.23; H, 7.93; and O, 23.84. IR spectra (ATR, ν/cm^{-1}): 2936, 2873, 1741, 1658, 1632, 1444, 1372,

https://doi.org/10.1021/acschemneuro.5c00862
ACS Chem. Neurosci. 2026, 17, 260−274

1230, 1026, 893. ^{1}H NMR ($CDCl_3$): δ 1.19 (s, 3H, 13-H_3), 1.27 (s, 3H, 14-H_3), 1.36 (s, 3H, 15-H_3), 2.02 (s, 3H, OAc), 2.03 (s, 3H, OAc), 4.95 (d, 2H, J = 3.2 Hz, 11-H_2), 5.02 (d, 1H, J = 11.0 Hz, 12-H) and 5.05 (d, 1H, J = 12.0 Hz, 12-H), 6.31 (s, 1H, 6-H). ^{13}C NMR ($CDCl_3$): δ 18.0 (C_2), 20.9 (C_{15}), 26.1 (both OAc), 28.8 (C_{13}), 32.3 (C_{14}), 34.9 (C_1), 37.4 (C_4), 40.2 (C_3), 44.2 (C_{10}), 55.6 (C_{11}), 57.5 (C_{12}), 124.0 (C_6), 128.9 (C_9), 167.3 (C_8), 171.1 (both $CH_3\underline{CO}$), 173.1 (C_5), 184.9 (C_7).

*11,12-Dihydroxydrim-8(9)-en-7-one (**7**) (72% Yield as White Crystals).* Mp 94.5−95.5 °C (from PE), $[\alpha]_D^{20}$ = +63.7 ^{0}(c 0.6). Found (%): C, 71.15; H, 9.34 O, 19.51. $C_{15}H_{24}O_3$. Calculated (%): C, 71.39; H, 9.58; O, 19.03. IR spectra (ATR, ν/cm^{-1}): 3321, 2923, 2851, 1658, 1442, 1318, 1001. ^{1}H NMR ($CDCl_3$): δ 0.91 (s, 3H, 13-H_3), 0.94 (s, 3H, 14-H_3), 1.18 (s, 3H, 15-H_3), 1.77 (dd, 1H, J = 3.7, 14.0 Hz 5-H), 2.41 (dd, 1H, J = 13.6, 17.0 Hz, 6-H) and 2.53 (dd, 1H, J = 3.4, 17.6 Hz, 6-H), 3.75 (br.s. 2H, OH), 4.32−4.51 (m, 4H, 11-H_2 and 12-H_2). ^{13}C NMR ($CDCl_3$): δ 18.3 (C_{15}), 18.4 (C_2), 21.2 (C_{14}), 32.4 (C_{15}), 33.0 (C_4), 34.8 (C_1), 35.1 (C_6), 40.2 (C_{10}), 41.0 (C_3), 49.9 (C_5), 56.1 (C_{11}), 58.0 (C_{12}), 134.6 (C_9), 161.6 (C_8), 201.2 (C_7).

*11,12-Dihydroxydrim-5,8(9)-dien-7-one (**8**) (70% Yield as White Crystals).* Mp 123−124.5 °C (from PE-Et_2O), $[\alpha]_D^{23}$ = +48.3 ° (c 0.5). Found (%): C, 71.78; H, 9.13; O, 19.09. $C_{15}H_{22}O_3$. Calculated (%): C, 71.96; H, 8.85; and O, 19.19. IR spectra (ATR, ν/cm^{-1}): 3361, 2964, 2935, 1650, 1614, 1461, 1391, 1003, 894. ^{1}H NMR ($CDCl_3$): δ 1.20 (s, 3H, 13-H_3), 1.28 (s, 3H, 14-H_3), 1.37 (s, 3H, 15-H_3), 4.36 (dd, 1H, J = 4.4, 11.7 Hz, 11-H), 4.49 (td, 2H, J = 2.4, 13.8 Hz, 11-H and 12-H), 4.65 (dd, 1H, J = 2.8, 11.7 Hz, 12-H), 3.62 (br.s. 1H, OH), 3.78 (br.s. 1H, OH), 6.31 (s, 1H, 6-H). ^{13}C NMR ($CDCl_3$): δ 18.0 (C_2), 24.7 (C_{15}), 28.3 (C_{13}), 32.3 (C_{14}), 34.1 (C_1), 37.6 (C_4), 40.3 (C_3), 43.7 (C_{10}), 56.1 (C_{11}), 58.5 (C_{12}), 124.0 (C_6), 128.9 (C_9), 165.9 (C_8), 174.0 (C_5), 187.1 (C_7).

*7-Keto-isodrimenine (**9**) (92% Yield as White Crystals).* Mp 117−118 °C (from PE), $[\alpha]_D^{21}$ = +36.9° (c 1.6). Found (%): C, 72.28; H, 8.01; O, 19.71. $C_{15}H_{20}O_3$. Calculated (%): C, 72.55; H, 8.10; and O, 19.35. IR spectra (ATR, ν/cm^{-1}): 2999, 2954, 2903, 2868, 1763, 1683, 1447, 1340, 1242, 1147, 1012, 783. ^{1}H NMR ($CDCl_3$): δ 0.91 (s, 3H, 13-H_3), 0.95 (s, 3H, 14-H_3), 1.27 (s, 3H, 15-H_3), 1.87 (dd, 1H, J = 2.9, 14.1 Hz 5-H), 2.62 (dd, 1H, J = 3.1, 7.6 Hz, 6-H), 2.66 (dd, 1H, J = 2.9, 5.3 Hz, 6-H), 4.81 (s, 2H, 12-H_2). ^{13}C NMR ($CDCl_3$): δ 17.8 (C_2), 18.0 (C_{15}), 21.0 (C_{13}), 32.7 (C_{14}), 33.1 (C_4), 33.2 (C_1), 36.0 (C_6), 36.7 (C_{10}), 41.0 (C_3), 51.9 (C_5), 67.2 (C_{12}), 149.0 (C_9), 152.4 (C_8), 170.8 (C_{11}), 196.3 (C_7).

*5,6-Dehydro-7-ketoisodrimenine (**10**) (82% Yield as White Crystals).* Mp 98−100 °C (from PE), $[\alpha]_D^{20}$ = +23.3° (c 0.27). Found (%): C, 73.29; H, 7.15; O, 19.56. $C_{15}H_{18}O_3$. Calculated (%): C, 73.14; H, 7.36; and O, 19.50. IR spectra (ATR, ν/cm^{-1}): 3506, 3302, 2996, 2958, 1720, 1555, 1484, 1429, 1327, 1167, 840. ^{1}H NMR ($CDCl_3$): δ 1.24 (s, 3H, 13-H_3), 1.32 (s, 3H, 14-H_3), 1.56 (s, 3H, 15-H_3), 4.95 (d, 1H, J = 17.6 Hz, 12-H), 5.02 (d, 1H, J = 17.6 Hz, 12-H), 6.39 (s, 1H, 6-H). ^{13}C NMR ($CDCl_3$): δ 17.6 (C_2), 23.9 (C_{15}), 27.7 (C_{13}), 32.7 (C_{14}), 34.3 (C_1), 38.2 (C_4), 40.9 (C_{10}), 41.0 (C_3), 67.4 (C_{12}), 124.8 (C_6), 149.5 (C_9), 149.6 (C_8), 170.7 (C_{11}), 176.9 (C_5), 182.4 (C_7).

*7-Acetoxy-isodrimenine (**12**) (90% Yield as White Crystals).* Mp 112−113 °C (from PE), $[\alpha]_D^{23}$ = +151.9° (c 1.1). Found (%): C, 70.08; H, 8.06; O, 21.86. $C_{17}H_{24}O_4$. Calculated (%): C, 69.83; H, 8.27; and O, 21.90. IR spectra (ATR, ν/cm^{-1}): 2953, 2928, 2868, 1753, 1736, 1455, 1372, 1232, 1046, 784. ^{1}H NMR ($CDCl_3$): δ 0.90 (s, 3H, 13-H_3), 0.94 (s, 3H, 14-H_3), 1.22 (s, 3H, 15-H_3), 2.11 (s, 3H, OAc), 4.56 (d, 1H, J = 17.4 Hz, 12-H), 4.63 (d, 1H, J = 17.6 Hz, 12-H), 5.56 (dd, 1H, J = 6.9, 10.1 Hz, 7-H). ^{13}C NMR ($CDCl_3$): δ 18.1 (C_2), 19.7 (C_{15}), 21.1 (OAc), 21.5 (C_{13}), 25.3 (C_6), 32.2 (C_{14}), 34.0 (C_1), 33.3 (C_4), 35.4 (C_{10}), 41.3 (C_3), 51.4 (C_5), 68.8 (C_{12}), 69.3 (C_7), 139.7 (C_9), 160.9 (C_8), 171.2 ($CH_3\underline{CO}$), 172.9 (C_{11}).

4.4. Electrophysiological Characterization of Novel Isodrimenine Derivatives at Human nAChR Subtypes. Human nAChR subunits were heterologously expressed in *X. laevis* oocytes to generate the following subtypes: $\alpha3\beta2$, $\alpha3\beta4$, $\alpha4\beta2$, $\alpha4\beta4$, $\alpha6^*\beta2\beta3$, $\alpha6^*\beta4$, $\alpha7$, $\alpha7\beta2$, and $\alpha9\alpha10$, as described previously.[22,23] Oocytes were injected with 5 ng of cRNA for $\alpha3\beta2$, $\alpha3\beta4$, $\alpha4\beta2$, and $\alpha4\beta4$ nAChRs, 10 ng of cRNA for $\alpha6^*\beta2\beta3$, $\alpha6^*\beta4$, $\alpha7$, and $\alpha7\beta2$ nAChRs, and 35 ng of cRNA for $\alpha9\alpha10$ nAChRs. For heteropentameric receptors, cRNA was injected at an α to α/β ratio of 1:1. Oocytes were obtained from 5-year-old female *X. laevis* (Nasco, Fort Atkinson, WI, USA), anesthetized with 1.7 mg/mL ethyl 3-aminobenzoate methanesulfonate (buffered to pH 7.4 with $NaHCO_3$). Oocytes were incubated at 18 °C in sterile ND96 buffer (in mM): 96 NaCl, 2 KCl, 1.8 $CaCl_2$, 1 $MgCl_2$, 5 HEPES, pH 7.4, supplemented with 5% FBS, 0.1 mg/mL gentamicin, and 100 U/mL penicillin-streptomycin.

Two-electrode voltage-clamp recordings were performed 2−7 days after cRNA microinjection using a HiClamp automated voltage-clamp screening system (MultiChannel Systems GmbH, Reutlingen, Germany) at a holding potential of −80 mV and room temperature (RT; 21−23 °C). Voltage-recording and current-injecting electrodes were pulled from GC150T-7.5 borosilicate glass (Harvard Apparatus, Holliston, MA, USA), filled with 3 M KCl, and had resistances of 0.3−1 MΩ. All procedures were approved by the Animal Ethics Committee of the Victor Chang Cardiac Research Institute and the University of Wollongong (project AE 20/17).

For $\alpha9\alpha10$-expressing oocytes, incubation with 100 μM BAPTA-AM [1,2-bis(2-aminophenoxy)ethane-*N*,*N*,*N*′,*N*′-tetraacetic acid tetrakis acetoxymethyl ester] at 18 °C for ∼3 h was performed before recording to minimize endogenous Ca^{2+}-activated chloride currents. Oocytes expressing $\alpha9\alpha10$ nAChRs were perfused (2 mL/min) with ND115 buffer (in mM): 115 NaCl, 2.5 KCl, 1.8 CaCl2, 10 HEPES, pH 7.4, whereas all other subtypes were perfused with ND96 buffer.

Receptor activation was tested with ACh applied at the half-maximal effective concentration (EC_{50}): 3 μM for $\alpha4\beta2$, 5 μM for $\alpha6^*\beta2\beta3$, 6 μM for $\alpha3\beta2$, $\alpha4\beta4$, and $\alpha9\alpha10$, 100 μM for $\alpha7$ and $\alpha7\beta2$, 200 μM for $\alpha6^*3\beta4$, and 300 μM for $\alpha3\beta4$. Oocytes were preincubated with each isodrimenine derivative (0.1−300 μM; prepared in ND96/ND115 + 0.1% BSA) for 5 min with the perfusion system paused followed by coapplication of ACh plus the compound under continuous flow. Controls with 0.1% BSA confirmed that neither BSA nor the perfusion pressure affected the nAChR activity.

4.5. Acetylcholine Concentration, Membrane Potential, and Deactivation Time Constant of Isodrimenine-Induced nAChR Inhibition. The inhibitory effects of DH7KID (15 μM) and 7KID (30 μM), concentrations close to their respective IC_{50} values, were further examined at $\alpha7$ and $\alpha4\beta4$ nAChRs. Inhibition was assessed across different ACh concentrations (30, 100, and 300 μM for $\alpha7$; 6, 30, and 100 μM for $\alpha4\beta4$), and at various holding potentials (−120 to −40 mV in 20 mV increments). Additionally, τ values were determined for $\alpha7$- and $\alpha4$-containing nAChR subtypes, calculated as the decay from peak current amplitude (evoked by ACh alone or ACh + compound) to baseline.

4.6. Data Analysis. Peak ACh-evoked current amplitudes were measured before (I_{ACh}) and during compound application ($I_{ACh+compound}$) using Clampfit software (version 10.7.0.3; Molecular Devices, San Jose, CA, USA). The relative current amplitude, expressed as $I_{ACh+compound}/I_{ACh}$, was used to quantify the compound activity at each nAChR subtype. Electrophysiological data (n = 6−10) are presented as mean ± standard deviation (SD).

Concentration−response relationships were fitted using the Hill equation in GraphPad Prism 9 (GraphPad, La Jolla, CA, USA) to determine IC_{50} values of the compounds, which are reported with 95% confidence intervals (CI). Statistical significance of inhibitory effects was assessed by Student's t test.

4.7. Molecular Docking and Molecular Dynamics Using nAChR Models. The 3D structure of the human $\alpha7$ nAChR (PDB code 7EKT)[24] was used for molecular docking and MD simulations. The unprotonated structure of DH7KID was generated using 2D Sketcher and LigPrep within Schrödinger Maestro (Version 12.5.139). Molecular docking was performed with QuickVina-W, following procedures described previously.[25] To estimate TBE values, the docked poses were rescored using the MM-GBSA protocol in Schrodinger Prime.[25] For each binding site, the conformer with the most favorable predicted binding affinity (i.e., lowest TBE) was selected for further analysis.

https://doi.org/10.1021/acschemneuro.5c00862
ACS Chem. Neurosci. 2026, 17, 260−274

The final docked conformers were subjected to MD simulations to assess stability.[25] Root-mean-square deviation values were measured across 300 ns trajectories, and averages were calculated from the last 100 ns. Poses with variance <0.5 were considered stable. MD simulations were prepared using CHARMM-GUI for membrane and script generation and executed with NAMD on the PETE supercomputer at the High Performance Computing Center (Oklahoma State University-Center for Health Sciences, Tulsa, OK).[26,27]

Final average TBE values and their SD were obtained using the Calculation of Free Energy (CAFE) plugin within the VMD molecular visualization program.[28,29] CAFE employs a rigorous thermodynamic cycle approach to estimate the binding free energies. From the last 100 ns of each 300 ns MD trajectory, 10 evenly spaced snapshots (n) were extracted and used for CAFE calculations to obtain the mean TBE and corresponding standard error (SE):

$$\mathrm{SE} = \mathrm{SD}/\sqrt{n} \tag{1}$$

The SE provides an estimate of the uncertainty in the mean TBE, indicating the precision of binding energy calculations derived from the sampled MD data. Conformers for which the upper confidence limit (mean + SE) of the TBE was positive were excluded as this indicated unfavorable binding free energy and unstable conformations.

4.8. Molecular Properties of Isodrimenine Derivatives. Physicochemical and ADME (absorption, distribution, metabolism, and excretion) descriptors for the isodrimenine derivatives were predicted using QikProp (Schrödinger, LLC). The reported parameters included the octanol/water partition coefficient (LogP; lipophilicity), PSA, solvent-accessible surface area (SASA), and its hydrophobic (FOSA), hydrophilic (FISA), and π contributions (PISA). Fh was calculated as

$$\mathrm{Fh} = \frac{\mathrm{FOSA}}{\mathrm{FISA} + \mathrm{FOSA}} \tag{2}$$

Although SASA also includes weakly polar contributions (WPSA), these were excluded from the Fh calculation to better capture the classical balance between the hydrophobic and hydrophilic character relevant to membrane partitioning. PISA was retained as a separate descriptor to quantify molecular surfaces capable of π-based interactions, such as $\pi-\pi$ stacking or π–alkyl contacts. Predicted permeabilities across model membranes were also evaluated: QPPCaco, which estimates passive permeability through human intestinal Caco-2 cell monolayers, and QPPMDCK, which is based on Madin-Darby Canine Kidney cells. Additional descriptors included aqueous solubility (PlogS) and predicted human oral absorption, both of which provide integrative measures of the passive permeability.

Compounds were considered more likely to partition into lipid bilayers when they met the following criteria: LogP between 1–4 (indicating moderate lipophilicity sufficient for membrane partitioning without compromising aqueous solubility), PSA < 90 Å^2 (indicating low polar surface), Fh ≥ 0.65 (reflecting a high fraction of hydrophobic surface), and QPPCaco ≥ 500 nm/s (indicative of high predicted passive permeability). LogP values outside this range either reduce membrane insertion due to excessive hydrophilicity (<1) or compromise solubility and bioavailability due to excessive lipophilicity (>4).[30−32]

AUTHOR INFORMATION

Corresponding Author

Han-Shen Tae − *Molecular Horizons/Faculty of Science, Medicine and Health, University of Wollongong, Wollongong, NSW 2522, Australia;* orcid.org/0000-0001-8961-7194; Email: hstae@uow.edu.au

Authors

Marcelo O. Ortells − *Facultad de Medicina, Universidad de Morón, MetaVitalic, and CONICET, Morón, Buenos Aires B1708, Argentina*

Alexandru Ciocarlan − *Laboratory of Chemistry of Natural and Biologically Active Compounds, Moldova State University, Institute of Chemistry, Centre Applied Organic Chemistry, Chisinau MD-2028, Republic of Moldova*

Aculina Aricu − *Laboratory of Chemistry of Natural and Biologically Active Compounds, Moldova State University, Institute of Chemistry, Centre Applied Organic Chemistry, Chisinau MD-2028, Republic of Moldova*

Lidia Lungu − *Laboratory of Chemistry of Natural and Biologically Active Compounds, Moldova State University, Institute of Chemistry, Centre Applied Organic Chemistry, Chisinau MD-2028, Republic of Moldova*

Svetlana Blaja − *Laboratory of Chemistry of Natural and Biologically Active Compounds, Moldova State University, Institute of Chemistry, Centre Applied Organic Chemistry, Chisinau MD-2028, Republic of Moldova*

David J. Adams − *Molecular Horizons/Faculty of Science, Medicine and Health, University of Wollongong, Wollongong, NSW 2522, Australia;* orcid.org/0000-0002-7030-2288

Hugo R. Arias − *Department of Pharmacology and Physiology, College of Osteopathic Medicine, Oklahoma State University Center for Health Sciences, Tahlequah, Oklahoma 74464, United States*

Complete contact information is available at: https://pubs.acs.org/10.1021/acschemneuro.5c00862

Author Contributions

H.-S.T.: Manuscript review and editing, data visualization and validation, performed electrophysiological experiments and, formal data analysis and curation. M.O.O.: Data visualization and validation, performed molecular docking and molecular dynamics simulations and, formal data analysis and curation. A.C.: Chemical synthesis of compounds, A.A.: Chemical synthesis of compounds. L.L.: Chemical synthesis of compounds. S.B.: Chemical synthesis of compounds. D.J.A.: Manuscript review and editing, supervision, resources, project administration and funding acquisition. H.R.A.: Original manuscript draft writing, project administration, funding acquisition and conceptualization.

Funding

This work was supported by the National Health and Medical Research Council (NHMRC Grant APP2014544), University of Wollongong, Australia (to D.J.A.), the Institutional Research Program of the State University of Moldova, (subprogram code 010601) (to A.A.), and by an OVPR Pilot/Seed Grant (Oklahoma State University Center for Health Sciences) (to H.R.A.).

Notes

The authors declare no competing financial interest.

ACKNOWLEDGMENTS

The authors gratefully acknowledge funding support provided by the National Health and Medical Research Council, the Institutional Research Program of the State University of Moldova, and the Office of Research of the Oklahoma State University Center for Health Sciences.

■ ABBREVIATIONS

nAChR,nicotinic acetylcholine receptor; ACh,acetylcholine; DH7KID,5,6-dehydro-7-keto-isodrimenine; 7KID,7-keto-isodrimenine; 7AID,7-acetoxy-isodrimenine; RT,room temperature; FBS,fetal bovine serum; EC50,half-maximal effective concentration; IC50,half-maximal inhibitory concentration; n_H,Hill coefficient; τ,deactivation time constant; RMSD,root-mean-square deviation; ECD,extracellular domain; TMD,transmembrane domain; CYD,cytoplasmic domain, TBE, theoretical binding energy; LogP (lipophilicity),octanol/water partition coefficient; PSA,polar surface area; SASA,solvent-accessible surface area; FOSA,hydrophobic contribution of SASA; FISA,hydrophilic contribution of SASA; PISA,π contribution of SASA; Fh,fraction of hydrophobic surface

■ REFERENCES

(1) Jansen, B. J.; de Groot, A. Occurrence, biological activity and synthesis of drimane sesquiterpenoids. *Nat. Prod. Rep.* **2004**, *21* (4), 449−477.

(2) Beckmann, L.; Tretbar, U. S.; Kitte, R.; Tretbar, M. Anticancer activity of natural and semi-synthetic drimane and coloratane sesquiterpenoids. *Molecules* **2022**, *27* (8), 2501.

(3) Aricu, A.; Ciocarlan, A.; Lungu, L.; Barba, A.; Shova, S.; Zbancioc, G.; Mangalagiu, I. I.; D'Ambrosio, M.; Vornicu, N. Synthesis, antibacterial, and antifungal activities of new drimane sesquiterpenoids with azaheterocyclic units. *Med. Chem. Res.* **2016**, *25*, 2316−2323.

(4) Lungu, L.; Cucicova, C.; Blaja, S.; Ciocarlan, A.; Dragalin, I.; Barba, A.; Vornicu, N.; Geana, E. I.; Mangalagiu, I. I.; Aricu, A. Synthesis of homodrimane sesquiterpenoids bearing 1,3-benzothiazole unit and their antimicrobial activity evaluation. *Molecules* **2022**, *27* (16), 5082−5096.

(5) Lungu, L.; Blaja, S.; Cucicova, C.; Ciocarlan, A.; Barba, A.; Kulcitki, V.; Shova, S.; Vornicu, N.; Geana, E. I.; Mangalagiu, I. I.; Aricu, A. Synthesis and antimicrobial activity evaluation of homodrimane sesquiterpenoids with benzimidazole unit. *Molecules* **2023**, *28* (3), 933−942.

(6) Arias, H. R.; Feuerbach, D.; Schmidt, B.; Heydenreich, M.; Paz, C.; Ortells, M. O. Drimane sesquiterpenoids noncompetitively inhibit human $\alpha4\beta2$ nicotinic acetylcholine receptors with higher potency compared to human $\alpha3\beta4$ and $\alpha7$ subtypes. *J. Nat. Prod.* **2018**, *81* (4), 811−817.

(7) Mineur, Y. S.; Mose, T. N.; Blakeman, S.; Picciotto, M. R. Hippocampal $\alpha7$ nicotinic ACh receptors contribute to modulation of depression-like behaviour in C57BL/6J mice. *Br. J. Pharmacol.* **2018**, *175* (11), 1903−1914.

(8) Morel, C.; Fernandez, S. P.; Pantouli, F.; Meye, F. J.; Marti, F.; Tolu, S.; Parnaudeau, S.; Marie, H.; Tronche, F.; Maskos, U.; Moretti, M.; Gotti, C.; Han, M. H.; Bailey, A.; Mameli, M.; Barik, J.; Faure, P. Nicotinic receptors mediate stress-nicotine detrimental interplay via dopamine cells' activity. *Mol. Psychiatry* **2018**, *23* (7), 1597−1605.

(9) van Goethem, N. P.; Paes, D.; Puzzo, D.; Fedele, E.; Rebosio, C.; Gulisano, W.; Palmeri, A.; Wennogle, L. P.; Peng, Y.; Bertrand, D.; Prickaerts, J. Antagonizing $\alpha7$ nicotinic receptors with methyllycaconitine (MLA) potentiates receptor activity and memory acquisition. *Cell. Signal.* **2019**, *62*, 109338.

(10) Virendrabhai, V. M.; Mehta, N. R.; Ram, K.; Patani, P. Potential nicotinic receptor antagonists: chemistry, rationale, and research roadmap. *J. Popul. Ther. Clin. Pharmacol.* **2025**, *32* (8), 1120−1137.

(11) Levin, E. D.; Cauley, M.; Rezvani, A. H. Improvement of attentional function with antagonism of nicotinic receptors in female rats. *Eur. J. Pharmacol.* **2013**, *702* (1−3), 269−274.

(12) Koltsa, M. N.; Mironov, G. N.; Malinovskii, S. T.; Vlad, P. F. Synthesis of drim-8(9)-en-7-one, drima-5,8(9)-dien-7-one, and their 11,12-dibromo derivatives from norambreinolide. *Russ. Chem. Bull.* **1996**, *45*, 208−214.

(13) Vlad, P. F.; Gorincioi, E. C.; Coltsa, M. N. Synthesis of 5,6-dehydro-7-oxoisodrimenin from drim-8-en-7-one. *Russ. Chem. Bull.* **2003**, *52*, 502−504.

(14) Vlad, P. F.; Popa, D. P.; Gorincioi, E. C.; Coltsa, M. N.; Mironov, G. N. Synthesis of 11-hydroxydrim-8(9)-en-7-one and 11,12-dihydroxydrim-8(9)-en-7-one from drim-8(9)-en-7-one. *Russ. Chem. Bull.* **1990**, *49*, 98−101.

(15) Kuryatov, A.; Olale, F.; Cooper, J.; Choi, C.; Lindstrom, J. Human $\alpha6$ AChR subtypes: subunit composition, assembly, and pharmacological responses. *Neuropharmacology* **2000**, *39* (13), 2570−2590.

(16) Koizumi, W.; Otsubo, S.; Furutani, S.; Niki, K.; Takayama, K.; Fujimura, S.; Maekawa, T.; Koyari, R.; Ihara, M.; Kai, K.; Hayashi, H.; Ali, M. S.; Kage-Nakadai, E.; Sattelle, D. B.; Matsuda, K. Determinants of subtype-selectivity of the anthelmintic paraherquamide A on *Caenorhabditis elegans* nicotinic acetylcholine receptors. *Mol. Pharmacol.* **2023**, *103* (6), 299−310.

(17) Lee, C. H.; Hung, S. Y. Physiologic functions and therapeutic applications of $\alpha7$ nicotinic acetylcholine receptor in brain disorders. *Pharmaceutics* **2023**, *15* (1), 31.

(18) Wu, Y. J.; Wang, L.; Ji, C. F.; Gu, S. F.; Yin, Q.; Zuo, J. The role of $\alpha7$nAChR-mediated cholinergic anti-inflammatory pathway in immune cells. *Inflammation* **2021**, *44* (3), 821−834.

(19) O'Connor, S. M.; Sleebs, B. E.; Street, I. P.; Flynn, B. L.; Baell, J. B.; Coles, C.; Quazi, N.; Paul, D.; Poiraud, E.; Huyard, B.; Wagner, S.; Andriambeloson, E.; de Souza, E. B. BNC210, a negative allosteric modulator of the alpha 7 nicotinic acetylcholine receptor, demonstrates anxiolytic- and antidepressant-like effects in rodents. *Neuropharmacology* **2024**, *246*, No. 109836.

(20) Thomsen, M. S.; Mikkelsen, J. D. The $\alpha7$ nicotinic acetylcholine receptor ligands methyllycaconitine, NS6740 and GTS-21 reduce lipopolysaccharide-induced TNF-α release from microglia. *J. Neuroimmunol.* **2012**, *251* (1−2), 65−72.

(21) Ciocarlan, A. From (−)-sclareol to norlabdane heterocyclic hybrid compounds. *Chem. J. Mold.* **2022**, *17* (2), 19−34.

(22) Arias, H. R.; Tae, H. S.; Micheli, L.; Yousuf, A.; Ghelardini, C.; Adams, D. J.; Di Cesare Mannelli, L. Coronaridine congeners decrease neuropathic pain in mice and inhibit $\alpha9\alpha10$ nicotinic acetylcholine receptors and $Ca_V2.2$ channels. *Neuropharmacology* **2020**, *175*, No. 108194.

(23) Tae, H. S.; Ortells, M. O.; Tekarli, B. J.; Manetti, D.; Romanelli, M. N.; McIntosh, J. M.; Adams, D. J.; Arias, H. R. DM506 (3-Methyl-1,2,3,4,5,6-hexahydroazepino[4,5-b]indole fumarate), a novel derivative of ibogamine, inhibits $\alpha7$ and $\alpha9\alpha10$ nicotinic acetylcholine receptors by different allosteric mechanisms. *ACS Chem. Neurosci.* **2023**, *14* (14), 2537−2547.

(24) Zhao, Y.; Liu, S.; Zhou, Y.; Zhang, M.; Chen, H.; Eric Xu, H.; Sun, D.; Liu, L.; Tian, C. Structural basis of human $\alpha7$ nicotinic acetylcholine receptor activation. *Cell Res.* **2021**, *31* (6), 713−716.

(25) Tae, H. S.; Ortells, M. O.; Yousuf, A.; Xu, S. Q.; Akk, G.; Adams, D. J.; Arias, H. R. Tabernanthalog and ibogainalog inhibit the $\alpha7$ and $\alpha9\alpha10$ nicotinic acetylcholine receptors via different mechanisms and with higher potency than the $GABA_A$ receptor and $Ca_V2.2$ channel. *Biochem. Pharmacol.* **2024**, *223*, No. 116183.

(26) Phillips, J. C.; Braun, R.; Wang, W.; Gumbart, J.; Tajkhorshid, E.; Villa, E.; Chipot, C.; Skeel, R. D.; Kale, L.; Schulten, K. Scalable molecular dynamics with NAMD. *J. Comput. Chem.* **2005**, *26* (16), 1781−1802.

(27) Wu, E. L.; Cheng, X.; Jo, S.; Rui, H.; Song, K. C.; Davila-Contreras, E. M.; Qi, Y.; Lee, J.; Monje-Galvan, V.; Venable, R. M.; Klauda, J. B.; Im, W. CHARMM-GUI Membrane Builder toward realistic biological membrane simulations. *J. Comput. Chem.* **2014**, *35* (27), 1997−2004.

(28) Humphrey, W.; Dalke, A.; Schulten, K. VMD: visual molecular dynamics. *J. Mol. Graph.* **1996**, *14* (1), 33−38.

(29) Liu, H.; Hou, T. CaFE: a tool for binding affinity prediction using end-point free energy methods. *Bioinformatics* **2016**, *32* (14), 2216−2218.

https://doi.org/10.1021/acschemneuro.5c00862
ACS Chem. Neurosci. 2026, 17, 260−274

(30) Jorgensen, W. L.; Duffy, E. M. Prediction of drug solubility from structure. *Adv. Drug Delivery Rev.* **2002**, *54* (3), 355−366.
(31) Lipinski, C. A.; Lombardo, F.; Dominy, B. W.; Feeney, P. J. Experimental and computational approaches to estimate solubility and permeability in drug discovery and development settings. *Adv. Drug Delivery Rev.* **1997**, *23*, 3−25.
(32) Veber, D. F.; Johnson, S. R.; Cheng, H. Y.; Smith, B. R.; Ward, K. W.; Kopple, K. D. Molecular properties that influence the oral bioavailability of drug candidates. *J. Med. Chem.* **2002**, *45* (12), 2615−2623.

https://doi.org/10.1021/acschemneuro.5c00862
ACS Chem. Neurosci. 2026, 17, 260−274